AD NUMBER: AD0872607

LIMITATION CHANGES

TO:

Approved for public release; distribution is unlimited.

FROM:

Distribution authorized to US Government Agencies only; Export Controlled; 29 Jul 1969. Other requests shall be referred to Chief, Air Force Technical Application Center, Alexandria, VA 22313.

AUTHORITY

USAF ltr dtd 3 Mar 1972

INVESTIGATION OF P TRAVEL TIME CURVE

29 July 1968

Prepared For
AIR FORCE TECHNICAL APPLICATIONS CENTER
Washington, D. C.

By
J. P. Everndon
Advanced Research Projects Agency
D. N. Clark
Seismic Data Laboratory

Under
Project VELA UNIFORM

Sponsored By
ADVANCED RESEARCH PROJECTS AGENCY
Nuclear Monitoring Research Office
ARPA Order No. 624

INVESTIGATION OF P TRAVEL-TIME CURVE

SEISMIC DATA LABORATORY REPORT NO. 236

AFTAC Project No.:	VELA T/9706
Project Title:	Seismic Data Laboratory
ARPA Order No.:	624
ARPA Program Code No.:	9F10
Name of Contractor:	TELEDYNE INDUSTRIES, INC.
Contract No.:	F33657-69-C-0913
Date of Contract:	2 March 1969
Amount of Contract:	$ 950,000 (Letter Contract)
Contract Expiration Date:	1 March 1970
Project Manager:	Royal A. Hartenberger (703) 836-7647

P. O. Box 334, Alexandria, Virginia

AVAILABILITY

This document is subject to special export controls and each transmittal to foreign governments or foreign nationals may be made only with prior approval of Chief, AFTAC.

This research was supported by the Advanced Research Projects Agency, Nuclear Monitoring Research Office, under Project VELA-UNIFORM and accomplished under technical direction of the Air Force Technical Applications Center under Contract F33657-69-C-0913.

ABSTRACT

By using a large number of LRSM stations and a number of earthquakes from all azimuths and the well-controlled nuclear explosions, a study of the "P" travel-time curve reveals it to be nearly a series of straight-lines or legs throughout the total distance of about 105°. Time as well as amplitude residuals were determined for the stations used and were found to be acceptably consistent. Analysis of the variance of the several modes of handling the data of each leg is shown which is significant in indicating the relative probability of each model as an explanation of the observed data. The "F" statistic value, degrees of freedom, etc. are shown for each leg. The existence of real differences in "P" travel-times and thus of mantle velocity structure are illustrated indicating that the velocity varies as a function of azimuth.

The very close correlation between site geology and average noise level on signal amplitude is discussed as well as this effect on magnitude calculations.

In addition, a computed "B-factor" curve developed from this study is compared with Gutenberg's and one by Clawson of Geotech.

TABLE OF CONTENTS

LIST OF TABLES

INTRODUCTION

There have been several procedures followed in investigations of the P travel-time curve. Gutenberg located numerous earthquakes by various techniques and plotted measured P phases for all earthquakes on one travel-time-versus-distance figure. He drew what seemed to be the best mean curve or curves through the somewhat scattered data. Jeffreys applied statistical theories to fundamentally the same approach, deriving a travel-time curve nearly identical to that of Gutenberg when using data of the same type and quality. Jeffreys' approach to generation of travel-time curves has been extensively elaborated upon by later investigators, reaching its culmination in recently reported work of Herrin. The travel-time curve published by Jeffreys-Bullen is a curve having no near-discontinuities over the epicentral distances from 0 to 105°. Extensive work by several investigators has made it clear that the P travel-time curve in the distance range 0 to 20° is highly variable over the earth and, in any region, is composed of a series of essentially straight line segments. Herrin, in his most recent work, has recognized this fact and, while publishing a travel-time curve for the distance range 0 to 20°, makes it clear that regional and near-regional travel-time curves must be devloped locally and that one cannot use a standard worldwide travel-time curve for locating seismic events when using regional and near-regional data. Herrin's teleseismic travel-time curve, though significantly different from that of Jeffreys-Bullen, also has no near-discontinuities present.

A basically different approach to investigation of the P travel-time curve is to limit each study to data of a single large earthquake or explosion. If this is done and

the data are analyzed azimuthally, the result is that the travel-time curve appears to be a series of straight lines, even at long teleseismic distances. Carder has persisted in such assertions for many years.

Extensive investigations of teleseismic data for numerous explosions at the Nevada Test Site (NTS) make it absolutely certain that the travel-time curve is a series of nearly straight line segments to a least 35°. Anderson and others have reported on this character and have used these data to demonstrate the existence of at least second order discontinuities in earth properties at depths of approximately 400 and 800 kilometers.

Historically, the two approaches of statistical treatment of data of many events versus detailed treatment of the data of a single event have proceeded in parallel. Those doing the statistical investigations have asserted that the existence of straight line segments could not be shown to be statistically necessary and that available travel-time data could not discriminate between the relative merit of the two types of travel-time curves. It is also relevant that the implications about mantle structure which follow from a travel-time curve composed of near-straight line segments are of such nature and possible complexity that one would rather not address the problem unless absolutely necessary. The result has been that the apparently clear demonstration of the nature of the travel-time curve derivable from individual events has been largely ignored by the geophysical community in favor of accepting the conclusions of the massive statistical data treatment. It is extremely important to determine which of these two types of travel-time curve best relates to the actual conditions within the mantle of the earth. It makes little

difference in the location of events, but it is profoundly significant relative to our understanding of the structure of the earth's mantle. In addition, there is high probability that the massive data treatment technique is effectively obscuring regional variations in mantle velocity structure.

The basic intent of this investigation is to strive for an optimum mix of seismological perception and statistical treatment in order to acertain which curve best describes the actual situation. In other words, the intent is to bring together the two modes of investigation followed for some decades into a single technique and to determine whether a further level of refinement and understanding of earth structure can be achieved. The shortcoming of an approach such as that of Herrin's is indicated by the high standard deviation of the observational data from his travel-time curve, even after applying station correction factors. The heterogeneities in the earth's crust, which have been demonstrated in earlier work, and the heterogeneities within the mantle, which will be here demonstrated to exist, are of such magnitude that a massive treatment of the total data of many earthquakes and explosions can only hope to get statistically close to the mean shape of the P travel-time curve. Such an approach cannot hope to ascertain the detailed shape and variations of the P travel-time curve.

TECHNIQUE OF INVESTIGATION

Our objective is to develop a technique of handling the data of many earthquakes and explosions which will eliminate the fundamental problems associated with treatments such as that of Jeffreys and Herrin. The approach followed has been to use the Long Range Seismic Measurement (LRSM) vans of the

VELA-UNIFORM research program as elements of a large US-wide array. The use of such data was dictated by the unusually high quality of these stations. Earthquakes were investigated which occurred during the time period when approximately 40 LRSM vans were widely distributed in an essentially fixed pattern over the US. An aperture of 2000 kilometers or more was available for each earthquake or explosion investigated. By limiting data used to that obtained within the US or the southern edge of Canada, errors in epicenter location, depth, and origin time would little affect an investigation of the shape of the P travel-time curve. Such errors would certainly affect the absolute value of travel-time but would not affect relative travel times to stations distributed in a small range of azimuth from the earthquake or explosion. A similar approach is being followed today by several investigators when determing values of $dT/d\Delta$ versus Δ from Large Aperture Seismic Array (LASA) data. However, the problem with LASA-based investigations is that the aperture used is so small that one may be led to attach worldwide significance to variation in $dT/d\Delta$ measurements which are simply a function of local structure in the vicinity of LASA. By use of large apertures, this factor hopefully will be eliminated and more valid estimates of $dT/d\Delta$ variations will result. The procedure followed was to:

a. Select a period of time when the LRSM vans were fully deployed across the US and were in a stable configuration (June 1963 - December 1964).

b. Search the entire file of LRSM data to find events with reasonably clear P phase starts as recorded in the US. The selection of earthquakes used was based upon this P phase criterion.

c. Select events at as many azimuths and distances from

the US as possible in order to allow investigation of the shape of the travel-time curve at all P range distances and as a function of azimuth of arrival. The large aperture employed insured extensive overlap of travel-time segments from earthquake to earthquake as mean epicentral distances of the earthquakes increased. Data of several earthquakes and explosions were plotted with the intent of determining the points of high $d^2T/d\Delta^2$. It was clear in this phase of the investigation that the travel-time curve was much more nearly a series of straight lines than any travel-time curve as yet publishied.

d. The data of each segment of the travel-time curve, segments of the travel-time curve being those portions between regions of high $d^2T/d\Delta^2$, were then investigated for curvature.

e. By use of available explosions data, surface focus travel-time curves were generated for the full P range distance.

f. Amplitude data of the same events were analyzed in a similar manner.

In order to merge the data of numerous events observed at numerous stations in the manner desired, both station correction factors and event intercept factors must be statistically estimated. A digital program was written which, given a body of travel-time data from numerous events observed by a fixed set of stations over a designated epicentral distance, would determine in the least squares sense the slope of the travel-time curve, individual station corrections factors, and event intercept factors. The pertinent equation is:

$t_{ijk} = a_j + b_k \Delta + s_i$ for station i, event j, and leg k.

The data of each leg of the travel-time curve were analyzed by use of this program. Only data from the western US (WUS) were analyzed in this manner as available data from the eastern US (EUS) were inadequate to allow valid operation of the matrix inversions involved in the computer program. Station correction factors determined from this program varied from leg to leg for each station. However, no clearly demonstrable patterns of systematic change as a function of distance was evident. Therefore, it was concluded that the best estimate we could make of station correction factors was to average the values determined for each leg, taking account of the quantity of data available for each leg. Another program was written which applied a given set of station correction factors to the travel-time data and estimated in a least squares sense the event intercept factors (a_j) and the coefficients of the travel-time curve (b_k) that best fitted the total data of each leg. With data from the EUS now included in the analysis, operation of the program was iterative as improved estimates of station correction factors were obtained. The criterion used for establishing final values of the station correction factors was that the mean residual over all legs of the travel-time curve for each station was essentially zero. Observed travel times were corrected for ellipticity and elevation of the stations to reduce the travel-time curve to that for the mean earth sphere. Thus, the station correction factors determined are due to crustal or mantle inhomogeneities below the stations. The following models were investigated for each leg of the travel-time curve:

a. $t = a + b\,\Delta$

b. $t = a + b\,\Delta + c\Delta^2$

c. $t = a + b\,\Delta + d\Delta^3$

RESULTS OF ANALYSIS

Table 1 presents the list of events studied and Figure 1 shows their location relative to the US. Table 2 indicates the LRSM stations employed in the investigation. These stations were so widespread and on such various rock types that an excellent opportunity was afforded for evaluating influence and relation of geology, geography, and noise level to time of arrival and amplitude of recorded signals. Table 3 is a tabulation of the station time anomalies determined by the procedures outlined above. These quantities vary from -1.07 seconds to +0.44 seconds. Figure 2 indicates the correlations between station location and measured time anomalies. In the WUS there is close correlation between the level of 1 second Rayleigh wave microseisms and computed station travel-time anomalies for P waves. Thus, the stations having noise levels between 0 and 5 millimicrons (HL-ID, WI-NV, MN-NV, EK-NV, CU-NV, KN-UT, and LC-NM) have a mean time anomaly of +.1 seconds, varying from -.1 to +.3. Stations with noise levels between 5 and 10 millimicrons (MV-CL, CP-CL, RT-NM, BX-UT, FR-MA, DU-OK, EB-MT, SK-TX, and RK-ON) have a mean time anomaly of -.5 seconds, varying from -.2 to -1.1 seconds. A similar correlation of noise level amplitude and P signal amplitude will be shown on page 27. It is clear that regional noise level measurements may be a much more subtle indication of crustal and upper mantle structure than we have realized previously. In such an interpretation, account must be taken of proximity to noise sources, etc. It should be pointed out that station correction or station travel-time anomalies of a second or more imply equivalent source correction factors relative to a mean worldwide travel-time curve. In most cases, available data are so limited that source anomalies cannot be accurately estimated.

It may well be possible to improve our understanding of the phenomena controlling these source and correction factors and thus learn to employ a mean worldwide travel-time curve in conjunction with a model of the required source and station correction factors.

The body of travel-time data was investigated in several ways. One procedure was to use the data of all events simultaneously for the determination of single values of the b, c, and d parameters of the travel-time curve models while computing individual event factors a_j. In addition, the data of each event were analyzed independently by the same travel-time curve models. The statistical results of such investigations are presented in the next series of tables. Table 4 gives travel-time curve coefficients and standard deviation of residuals when all data on each leg were treated simultaneously. The leg designations on all tables are the apparent surface velocity of the straight line model when using all data. Note that when using the travel-time criterion involving a Δ^2 or Δ^3 term, positive values of c and d were obtained for 3 segments of the travel-time curve. These values are quite certainly inadmissible. The lack of change in the standard deviation of residuals between the Δ^2 and Δ^3 models implies the total lack of significance of investigating both of these models. In the remainder of the investigation, only the Δ^2 model is considered.

Table 5 presents coefficients of the travel-time curve and standard deviations when using all data recorded from earthquakes located to the northwest of the US. In this situation, only one segment of the travel-time curve is computed to have a positive b value. Table 6 presents a similar analysis for all data recorded from earthquakes located to the south of the US. Table 7 presents similar

coefficients when all data of two travel-time legs were fitted to one common equation. Analysis of variance investigations indicated that in all cases there was low probability that the determined differences in standard deviation by the data handling techniques of Tables 3 and 7 were the result of random error. In all cases, the two-leg analysis was rejected.

Analysis of the variance of the several modes of handling of the data of each leg is significant in indicating the relative probability of each model as an explanation of the observed data. Table 8 presents the results of such analysis. In that table the several modes of handling of the data are indicated as follows:

a. "All $(a + b \Delta)$" implies all data analyzed according to travel-time curve $t = a + b \Delta$.

b. "All $(a + b \Delta + c\Delta^2)$" implies all data analyzed according to travel-time curve $t = a + b \Delta + c\Delta^2$.

c. "E $(a + b \Delta)$" implies data of each event analyzed according to travel-time curve $t = a + b \Delta$.

d. "E $(a + b \Delta + c\Delta^2)$" implies data of each event analyzed according to travel-time curve $t = a + b \Delta + c\Delta^2$.

The F statistic value, the degrees of freedom, and the resultant probability value are indicated in Table 8. Thus, for the leg designated 12.5, there is only an 0.005 probability that the decrease in standard deviation of residuals when analyzed by E $(a + b \Delta)$, relative to that for all $(a + b \Delta + c\Delta^2)$, is to be explained by chance. There is only an 0.05 - 0.10 probability that the differences between the standard deviations for E $(a + b \Delta + c\Delta^2)$ and E $(a + b \Delta)$ are not real. A summary of Table 8 is presented in the tabulation below. In that tabulation, an arrow indicates that the modes of analysis to the left of the arrow have a low (.10 or less)

probability of not being better modes of analysis than those to the right of the arrows. A swung dash (~) between the symbols for two modes of analyzing the data implies greater than .10 probability that the determined differences in values of standard deviation of residuals are the result of chance.

Leg Designator

12.5	$E(a + b\,\Delta + c\Delta^2) \rightarrow E(a + b\,\Delta) \rightarrow All(\Delta^2) \rightarrow All(\Delta)$
13.4	$E(a + b\,\Delta + c\Delta^2) \sim (.15)\ E(a + b\,\Delta) \sim All(\Delta^2) \rightarrow All(\Delta)$
14.5	$E(a + b\,\Delta + c\Delta^2) \sim E(a + b\,\Delta) \rightarrow All(\Delta^2) \sim All(\Delta)$
16.3	$E(\Delta^2) \sim E(\Delta) \sim All(\Delta^2) \rightarrow All(\Delta)$
18.2	$E(\Delta^2) \rightarrow E(\Delta) \sim All(\Delta^2) \rightarrow All(\Delta)$
19.5	$E(\Delta^2) \sim (.15)\ All(\Delta)$
22.0	$E(\Delta^2) \sim (.15)\ All(\Delta^2) \rightarrow All(\Delta)$
24.4	$E(\Delta^2) \sim (.15)\ E(\Delta) \rightarrow All(\Delta^2) \rightarrow All(\Delta)$

Thus, on all of the travel-time curve segments, there is 0.15 probability or less that the decrease in standard deviation resulting from individual event analysis relative to that for all event analysis occurs by chance.

Table 9 indicates in a somewhat different form the same results. In that table, the values of standard deviation for single event analysis, as well as for all data analysis, are presented, single event data being presented only when four or more stations were present on a leg. The relevant equation and mode of analysis are indicated in all columns. On Leg 12.5, while the standard deviation for all events analyzed according to All(a + b Δ) was .345 seconds, individual event values of standard deviation were in general much smaller (.121, .140, .277, .373, and .221). Inspection of each

segment of the travel-time curve reveals a similar relationship between standard deviations for individual events and standard deviation for all data. The implication, of course, is that the mean slope for at least the shallower travel-time curve segments is variable. This point will be returned to shortly. Table 10 indicates the "All" and "Individual" Event values of the travel-time curve parameters. Note the highly erratic behavior of the "c" coefficient for Individual Event analysis. This variability is so high, both plus and minus values being obtained, that one would not feel justified today in attaching significance to the detailed values here determined. This high variability also suggests that some of the decrease in standard deviation observed between $E(a + b\,\Delta)$ and $E(a + b\,\Delta + c\Delta^2)$ may not be as meaningful as regards nature of the travel-time curve as straight statistical analysis of Table 8 would suggest.

Table 11 is a tabulation of the determined values of the coefficient of Δ^2 (c) listed in previous tables. They are ordered so as to allow easier comparison of values determined with different data sets. It is uncertain whether much significance should be attached to a detailed comparison of these results. Thus, can one believe that, on Leg 13.4, the travel-time curve may have reversal of curvature depending upon the direction of arrival of the waves? Similarly, can one believe the relative values obtained for northwest and south data on Leg 19.5? The determined values of c from leg to leg are quite variable. Using as basis of discussion the average of values determined for northwest and south data, "c" values range from essentially zero on the 14.5 leg ($+0.23 \times 10^{-6}$) to -2.9×10^{-6} on the 16.3 leg. The mean value of "c" for all legs is -1.37×10^{-6}.

Before proceeding to a discussion of the derived travel-time curve, we will demonstrate that slope differences as determined by using waves crossing the US in different directions are, for some legs, distinctly different in a statistical sense. The equation used for this investigation is the linear curve, i.e., $t = a + b\,\Delta$. Table 12 presents the values of the "t" statistic and "P" resulting from straightforward analysis of the data.

There is very low probability that the mean slope of the 12.5 leg is the same for waves propagating north and south relative to those propagating east and west. For the 13.4 leg ,the data indicate no statistically strong basis for assuming variations in mean velocity for north and south propagating waves. However, on the 14.5 leg, there is clear indication of different slope values, as there is also on the 18.2 leg. The limited data available for other path directions across the US (see Table 10 for data of Atlantic and Hawaiian earthquakes) supports the variability of velocity at this level in the mantle. Deeper legs show no strong evidence of differences in apparent velocity across the US. The apparent reality of the differences of slope on the 18.2 leg imply regional variations in velocity structure to depths of at least 1900 kilometers in the mantle (see Figure 11).

TRAVEL-TIME CURVES

The generation of a travel-time curve from data such as these requires a step in analysis beyond that so far described. The nature of the data available required the estimation of the travel time for a surface focus event on several legs of the travel-time curve for which no data of a surface focus event were available. The procedure was to begin the

travel-time curve on a leg where surface focus events were available, the leg chosen being the 12.5 leg which included data of numerous NTS explosions. Little or no explosion data were available for the 13.4 leg, but several earthquakes were observed on both the 12.5 and 13.4 legs. The event intercepts ("a" values) for these several events on the 12.5 let were subtracted from the mean NTS intercept. These intercept differences were then added to the appropriate event intercept values on the 13.4 leg and the resultant set of computed surface focus intercept values averaged. Given this intercept and the computed slope of the travel-time curve on the 13.4 leg, the total travel-time along this leg for a surface focus event was thus established. Estimation of the travel-time curve for more distant legs continued in similar manner. At great distances, travel-time data from 3 surface focus sites became available and comparison between observed travel-times and those predicted by the scheme outlined above became possible. Curve EC-CU-I was completed on the last two legs by controlling intercept values by Semipalatinsk data rather than by the procedure outlined above. Table 13 indicates the straight line travel-time curves computed from various data sets along with comparison with explosion data. The asterisk on all intercept values for the 12.5 leg indicate that these values are controlled by NTS data. The double asterisk for the entry on the 22.0 leg under South data implies that the control on that intercept is the Northwest data. The reason for this procedure will be apparent shortly. Values in parentheses on South data indicate the values of intercept that are to be associated with South data if the slope determined from Northwest data is employed, these entries in the table being solely to allow rapid intercomparison of the 2 determined travel-time curves. The

entries for explosion data are all calculated against the slopes determined for Northwest data. A comparison of the northwest travel-time curve and the explosion data yields the intercept differences shown in the final column. The travel-time curve determined by extrapolation from the 12.5 leg agrees well with Novaya Zemlya and Algerian data on the 16.3 and 18.2 legs. However, there appears to be a real and systematic difference in mean slopes of the travel-time curves between the 16.3 and 24.5 legs as computed by our extrapolation procedures and as determined from empirical observations based on the seismic signals at Novaya Zemlya, Semipalatinsk, and Algeria. This problem is not removed at all if a travel-time curve is developed based on the equation $t = a + b\,\Delta + c\Delta^2$. It is difficult to understand how the scheme followed in development of the curve would so systematically depart from the "actual" curve if available explosion data is really indicative of the "actual" curve. It may be more reasonable to assume that this systematic difference is expressive rather of path influences than of error in mode of calculation.

A puzzling circumstance developed between the travel-time curves based on northwest and south data. In Table 13, at leg 14.5, there are two entries. The upper one $(156.9 + 0.06788\,\Delta)$ is derived by legwise extrapolation from the 12.5 leg, while the lower equivalent entry $(159.6 + .06788\,\Delta)$ is derived by legwise extrapolation from 22.0 leg. When the attempt was made to estimate continuously from the 12.5 leg through the 14.5 to more distant legs, shallow focus earthquakes were observed to have travel-times greater than the computed surface focus travel-time curve. This entire problem was associated with the 14.5 leg. Extension from the 22.0 leg (using intercept on 22 leg of Northwest data as control) to the

16.3 leg yielded estimates of travel-time in agreement with the Northwest data and with the analysis based on All data. Similarly, the travel-times estimated for the 13.4 leg from the South data agree well with those derived for the Northwest data. The nature of the problem in the 14.5 segment of the travel-time curve is uncertain at this time.

The final computed travel-time curves (EC-CU I and EC-CU II) were obtained by plotting individual station residuals for all data against the computed straight line segmented travel-time curve (EC-SL I and EC-SL II) and subsequently drawing a curve under certain assumptions mentioned below through these plotted data points. Figure 3 through 10 were thus obtained. On all figures, the Jeffreys-Bullen and HERRIN-67 travel-time curves are shown. It is clear that the "best" curve through the data points differs markedly from both of these curves. In fact, the data essentially support the idea of near-straight line segments. Such a travel-time curve, however, is not appropriate for normal inversion schemes designed to determine velocity structure in the mantle. Therefore, the approach followed was to ignore large positive residuals at the ends of each leg, thus allowing the drawing of a more smoothly changing travel-time curve through the remaining points. This was, of course, somewhat illogical but was necessary to allow appreciable distances for curvature changes. Any velocity structure determined for the earth by use of this travel-time curve probably will be more smoothly changing than the actual case.

EC-CU I is the curve so labeled on Figures 3 through 10. The reason for the discrepancy in the distance range 3000 to 7000 between that curve and HERRIN-67 is uncertain but did suggest that it might be well to compute another.

That curve, EC-CU II, was obtained by using the legwise shapes of EC-CU I but using an average travel time on each leg equal to the mean travel-time for the same distance range on the HERRIN-67 curve.

Table 14 is the straight line segmented curve of Figures 3 through 10, EC-SL I. The regional and near-regional portions of the travel-time curve of Table 14 are arbitrary and approximately expressive of conditions in eastern North America. Table 15, curve EC-SL II, is the straight line segmented travel-time curve with mean travel-time on each leg equal to mean time over the same distance range on the HERRIN-67 curve. Table 16, curve EC-CU I, is the curved travel-time representation of Figures 3 through 10, while Table 17, curve EC-CU II, is as described above.

All curves were sent to G. Clawson of Geotech who inverted them and provided us with the velocity versus depth relationship for the earth's mantle. Some smoothing of teleseismic portions of the curve were required in order to remove apparent discontinuities and low velocity (straight line portions of travel-time curve) layers. As noted above, this is a stricture on all inversions schemes. If the travel-time curve appears to suggest such characteristics, they will not appear in the answer since the effect will be removed in the process of adjusting the data for inversion. Even so, the resultant velocity versus depth curve is strongly suggestive of near-discontinuities in the velocity structure or at least of rapid changes in dT/dz. Figure 11 presents the determined velocity versus depth function for EC-CU II. There seems little doubt, particularly in light of the nature of the discrepancy between individual event analysis and all data analysis mentioned above, that the velocity versus depth as determined is significantly smoother than is

the actual situation in the mantle. In fact, on Figure 11 the presence of intervals of rapid change of velocity in the mantle are clearly suggested if straight lines are drawn as shown through the plotted velocity versus depth points.

DATA ON REGIONAL VARIATION OF MANTLE STRUCTURE

We have already mentioned the statistical analysis of the northwest, south, and NTS data which clearly implied the existence of real travel-time differences, both as regards slope and travel time, at several depths down to 1900 kilometers in the mantle of the earth. Analysis of the individual event data of Tables 8, 9, and 12 statistically supports the reality of marked differences in mantle velocity structure.

The existence of real differences in P travel-times and thus of mantle velocity structure are illustrated by the individual event data of Figures 12 through 16. The data of these figures are analyzed by use of mean velocity values for All data rather than by using the individual event values of Tables 9 and 10. With one exception, each figure shows data for two events located at nearly opposite azimuths relative to the US. Figure 12 compares a Kamchatka event with one from Bolivia, both events occurring at approximately the same depth. The figure indicates about a 0.7 second difference in relative travel times between the two curve segments shown for the two events. This relative difference can only indicate that velocity structure in the mantle varies as a function of propagation path to the US. The data used on all of these figures is of such quality that the relative times are known to much better than 0.7 seconds. Therefore, it is impossible to explain the 0.7

second difference by reinterpretation of the data of the figure. Possible errors in origin time, location, and focal depth cannot be such as to make the data of these two events imply the same velocity structure. Figure 13 compares the data of the same Kamchatka earthquake with that of an earthquake on the southerly Atlantic Ridge. The relative time difference between the data of these earthquakes is greater than for the previous pair, being 0.8 seconds. Relative time differences are comparable for the data of Figures 14 and 15 which compare events from Honshu and Chile and from Peru and the Aleutian Islands. Figure 16 compares the reduced travel-time curve data for two events from the same area (Kamchatka), indicating that data of two such events imply the identical mantle velocity structure.

Additional evidence for the existence of mean travel-time discrepancies, as recorded in the US from seismic signals in Novaya Zemlya, Semipalatinsk, and Algeria, is provided by considering the following data:

a. Travel-times from Eniwetok to the US (80° to 100° epicentral distances) were essentially identical to those for continent-to-continent travel times, thus implying that no systematic increase or decrease in long distance teleseismic travel times is associated with oceanic source regions.

b. Observed travel times on the 12.5 leg for a near-surface explosion in the Atlantic (CHASE III, exploded at depth of 900 feet in water depths of 6000 feet) were only slightly greater (+0.4 seconds) than were travel times at the same distance range from explosions at NTS. The travel times for CHASE II (exploded at a depth of approximately 4500 feet in water depths of 9000 feet) were 0.5 seconds

less than travel times at similar distances for NTS explosions. If CHASE II had been exploded at the surface, observed travel times on the 12.5 leg would have been greater by approximately 1 second than those observed at similar distances from NTS explosions, all recording stations being within the eastern US as defined in Evernden 1967[1]. The slow propagation velocity of sound in water compared to that in rock suggests that velocity in the upper mantle must either be faster under oceans than under continents or that the rapid velocity change interval associated with the 12.5 leg is at shallower depth under the ocean than under the continents.

c. When shallow focus earthquakes on the mid-Atlantic ridge are located by use of the HERRIN-67 travel-times curve and observing stations are at distances of 25 to 140°, the computed solution generally is above ground or at least well above the pP depth, this result being particularly strong if PKP data are included. The implication of this result is that the actual travel-time curve for events on the mid-Atlantic ridge has a greater mean slope between 25° and 100° than does the HERRIN-67 curve. A uniform increase or decrease of travel-time at all distances would not be detectable and would have no influence on depth calculations.

It cannot be positively determined from these data alone whether the explanation is to be found in abnormally short travel times at short teleseismic distances or in abnormally long travel times at long teleseismic distances. However, the three items above suggest the former. Explanation of the

---

[1] Evernden, J.F., Magnitude Determination at Regional and Near-Regional Distances in the United States, Bulletin of the Seismological Society of America, Vol. 57, No. 4, pp. 591-639, August 1967.

CHASE data based on simply increasing velocity in the upper mantle while keeping the zone of high rate of change of velocity associated with the 12.5 leg at the same depth will not explain the mid-Atlantic ridge data. The apparent explanation of these three sets of data is one which places the zone of rapid change of dT/dz at a shallower depth under oceans than under continents. The change in depth of this zone required to explain the travel-time data is of the order of several kilometers.

Additional evidence of the reality of travel time differences at long teleseismic distances is provided by comparison of the accuracy of locations obtained by use of the LRSM data of this report and travel time curves EC-CU-I and EC-CU-II. Remember that EC-CU-I is based solely on data of this report and certain previously discussed procedures for estimating the travel-time curve at all distances by using control data at short distances. This procedure was abandoned, unfortunately (as will be indicated below), for the two more distant legs. EC-CU-II was constructed to yield agreement with HE-67 on the average on all legs. The two curves are systematically different from 20° to 80°. When locating events by use of worldwide data, the systematic differences between these two curves will have little effect on computed locations (Table 18) but may significantly effect depth calculations. As a matter of fact, HE-67 and EC-CU-II yielded depths in better agreement with pP than did EC-CU-I when using worldwide data.

However, when locating events by use of data obtained in limited azimuth and range, the location is markedly influenced by the exact shape of the travel time curve. When using worldwide data, i.e., stations at many azimuths and distances from the epicenter, the location program effectively uses total travel time in the computations. In contrast, when

using data obtained only in a limited azimuth range, the location program essentially fits the observations to the shape of the travel time curve used. Total travel time is not effectively analyzed, only the shape of the observed data. Thus a small systematic error in shape of the travel time curve versus distance will not significantly affect computed locations when using worldwide data but may markedly affect locations when all observations are within a narrow azimuth range. The rate of change of slope of the P travel time curve, particularly for segments of 2,000 kilometers or more in length, is so gradual that even small changes in mean slopes will cause significant shifts in the computed epicenters.

The evaluation of the relative accuracy of locations obtained by use of EC-CU-I and EC-CU-II and US-observations is determined by the comparison of locations obtained by the two curves with that obtained with worldwide data. Size and orientation of the 95% CHI^2 ellipse (s.d. = 0.4) are also shown. The relation between tectonic structural trends and US-epicenter directions is so variable for the 12 events used in Table 20 that location bias problems cannot significantly affect the interpretation. For the 12 events of Table 20 the semi-major axis of the 95% CHI^2 ellipse (s.d. = 0.4 seconds) is less than 60 km and the travel time data were obtained almost entirely in those portions of the two travel time curves which are systematically different. All locations calculated were restrained to the depth indicated either by pP or by worldwide data computations. The standard deviation 0.4 seconds is established by averaging the standard deviation values obtained for all events studied.

Table 19 presents comparison of locations by EC-CU-I and EC-CU-II for 31 events while Table 20 presents the pertinent comparison data for the 12 events described above. It can be seen from Table 20 that, on the average, the locations as computed by EC-CU-II were 40 km too far from the United States while locations computed according to EC-CU-I were only 1 km too far. Thus, it is immediately apparent that when locating events by use of data obtained in a limited azimuth and range with the US, curve EC-CU-1 is distinctly superior to curve EC-CU-II. The authors of this paper do not pretend to assert that EC-CU-I is better for a worldwide travel time curve than HE-67; in fact, they believe quite the opposite. The point being demonstrated is that the variations in mantle velocity structure and thus in teleseismic travel time are real and, at least to the extent here demonstrated, indicate the necessity of developing regionally calibrated travel time curves.

LONG SHOT DATA

The anomalous nature of the travel-time data for LONG SHOT, a nuclear explosion on Amchitka Island in the Aleutians, is apparent when related to the data of this report. Only a handful of the LRSM stations occupied during 1963-1964 were still in operation at the time of LONG SHOT but sufficient data are available to illustrate its anomalous character. The slopes and intercepts of the travel time curves derived in this report, particularly curves computed solely by use of events to the north and west of the US, are in large part based on shallow focus Aleutian Island earthquakes. None of these events showed marked discrepancy from the others in the same area as regards standard diviation of the residuals or computed values of intercept for simulated surface focus travel-time curves.

The following table indicates intercept values computed on the northwest surface focus travel time curve by use of earthquakes as well as indicating comparisons with Novaya Zemlya, Alergia and LONG SHOT data.

COMPARISON OF NORTHWEST EARTHQUAKES AND LONG SHOT DATA

Leg Designation	Northwest Surface Focus Travel-Time Intercept	Novaya Zemlya and Algerian Intercept ($dT/d\Delta$ controlled by NW earthquakes)	LONG SHOT Intercept ($dT/d\Delta$ controlled by NW earthquakes)
14.5	149.2	--	148.2 (3 stations, MV-CL, CP-CL, RK-ON)
16.3	197.5	196.9 - NZ 197.2 - ALG	196.1 (2 stations, LC-NM, GV-TX)
18.5	253.0	253.2 - NZ 253.5 - ALG	249.7 (2 stations, DH-NY, HN-ME)

The standard deviation of residuals for the LONG SHOT data on the 14.5 leg was 1.1 seconds. They were small on the last two legs (stations close together) but would be very large (1.5 seconds) if all LONG SHOT data were computed against the northwest travel-time curve using the 3 distance legs simultaneously. As noted above, the values of the the northwest intercepts are controlled largely by shallow focus Aleutian Islands earthquakes, none of which show anomalous intercept values similar to those of LONG SHOT data. These results would seem to indicate that the abnormal conditions causing

the observed pattern of LONG SHOT travel times are greatly restricted either in area or in depth near Amchitka. One of us has noted previously that master-controlled travel-time corrections derived from a nearby large shallow focus earthquake did not decrease standard deviation of LONG SHOT travel times. In other words, the detailed pattern of travel times observed for LONG SHOT are not typical of shallow mantle conditions 100 kilometers southwest of LONG SHOT (location of master event). Since master-controlled corrections to observed travel times markedly decrease standard deviation of residuals for well recorded earthquakes surrounding a master event, the failure of residuals of an event in an island arc area to decrease may imply an extremely shallow focus event.

Associated with this recognition of the existence of mantle velocity variations must come recognition of the step required in seismological observations in order to elucidate the details of this variation. Presently available regional networks are probably inadequate for these purposes due to variations in quality and character of records. Seismologists can obtain the necessary data if:

a. They pool their available resources with the intent

of operating on a temporary basis (2 years or so) networks of LRSM-quality stations on different continental regions with the intent of observing the details of mantle velocity structure. This network would be moved to different regions every couple of years, involving what might be called a Seismological Decade of international cooperation. Under the proper organizational arrangements, it might even be possible to obtain LRSM equipment.

b. They cooperate in establishing a worldwide network of a limited number of 200K-500K stations.

c. They attempt to obtain government support for ocean-bottom seismological installations whose purpose would be to obtain teleseismic data.

If seismologists would enter into such a cooperative self-help program, we are certain that significant advances in seismology would result. Efforts are generally too scattered and fragmentary to yield the data required. Only concerted effort allowed acquisition of the data here employed. The events investigated would be of such size that a well distributed worldwide network of two dozen reasonably capable stations would allow epicenter locations essentially as accurate as those obtainable by use of a hundred or more stations.

INVESTIGATIONS OF AMPLITUDE DATA

The original stimulus for this phase of the investigation was the desire to relate amplitude measurements (defined as the maximum amplitude of the Pn or P phase within the first three cycles of motion) to the travel-time curve with the intent of ascertaining whether the amplitude data would or would not support a near-segmented nature of the travel-time

curve and to make a new estimate of the shape of the B-factor curve. The same programs used in the analysis of the travel-time-versus-distance data were also used for the analysis of amplitudes versus distance, the relevant equation now being:

$$\log (\text{amplitude})_{ijk} = \alpha_j + \beta_k \log \Delta ij + s_i \quad \text{(station i of event j on leg k)}$$

Event factors (α_j) and station correction factors (S_i) were estimated by the least squares program. The β_k factors were similarly estimated, one for each segment of epicentral distance, the segments being established by the time-versus-distance analysis discussed above.

An interesting aspect of the analysis is the set of station amplitude anomalies and station correction factors and their relationship to geographic positions of the stations, noise levels at the stations, and the travel-time anomalies and correction factors at the stations. As can be seen in Table 21, virtually a full order of seismic magnitude of relative station amplitude corrections was computed. For such relative amplitude factors to be accepted as valid, it is virtually required that they show strong regional correlation and strong correlation with other determinable signal or station characteristics. The regional correlation is as shown in Figure 17, with amplitudes recorded in the WUS approximately 3 times (0.5 magnitude) lower than those recorded in EUS for P teleseismic signals. It has long been known that there is also a correlation between microseismic noise levels and geography in the US, stations in WUS generally having lower noise level than those in EUS. Noise level measurements previously made and published allow a detailed comparison of the estimated relative amplitude factors of this report and measured noise levels at the LRSM stations. The noise

measurements used are those made at Geotech. Their technique was to measure the maximum amplitude on the record within the P signal passband during the 10 seconds prior to a minute and to make such measurements over an extended period of time. The noise amplitude data were then plotted on a cumulative percent curve and the tabulated noise level for the station was the 50% point on this curve. Table 21 lists the relative amplitude (mμ) measurements determined from teleseismic P signals and the noise levels (mμ) as recorded by Geotech. Table 2 gave location and geological environment of each of the LRSM stations. Figure 18 is a plot of noise level versus relative signal amplitude for all LRSM stations used and the VELA observatories. The symbol for each station is keyed to its geology. Similar to Figure 18, Figure 19 is a plot of signal-to-noise versus noise ratio.

If, for the moment, we consider only those stations located on granitic or metamorphic rocks, it is seen that there is very nearly linear relationship between log N and log S on Figure 18 and between log N and log S/N on Figure 19. The point for Campo, California (CP-CL) is the only one showing a departure of more than a factor of 1 1/2 from this straight line. The abnormally high noise level is probably due to the station's proximity to the Pacific Ocean (Figure 17). Figures 18 and 19 clearly demonstrate the close correlation of noise level and P teleseismic signal level at these stations, the signal-to-noise ratio being greatest at stations with the lowest noise level. Figure 18 confirms that noisy stations generally have higher signal amplitudes for stations in the same geological environment, but Figure 19 indicates that quiet sites have higher signal-to-noise ratios.

The limited data available suggest that stations on limestone in the EUS may have signal levels below those of stations on granite, while no such difference in signal is detectable between limestone and granite stations in WUS. Stations on hard sandstone (Paleozoic and Mesozoic sandstones) appear to have consistently higher amplitude signals and higher signal-to-noise ratios than do stations in the same general area located on granite. Stations such as HH-ND, RY-ND, and GI-MA, situated on thick Tertiary and Cretaceous sediments, have abnormally high signals and signal-to-noise ratios for their noise level. The explanation for this phenomenon apparently must reside in the different influence of such thick, somewhat unconsolidated sediments on Rayleigh waves (the dominant noise source) and P teleseismic signals.

The analysis discussed above was based upon the teleseismic P signals of approximately 50 earthquakes recorded at all teleseismic distances from the US. In order to indicate the reality of the determined station amplitude factors in another way, 4 events not used in the analysis above were investigated in terms of the amplitudes of their P signals recorded in WUS and EUS. The data for these 4 events were published previously in Evernden, 1967.

UNADJUSTED MAGNITUDE VALUES (GUTENBERG B-FACTOR)

Event	$m_{teleseismic}$ (WUS)	$m_{teleseismic}$ (EUS)
Manzanilla 2 Feb 62	4.35 (16)*	4.77 (7)*
GNOME Explosion	3.9 (2)	4.4 (2)
SALMON Explosion	4.2 (13)	4.6 (5)
SS VILLAGE (CHASE II)	4.2 (13)	4.7 (4)

*Numbers in parentheses indicate number of stations.

Thus, results obtained by the analysis described above are supported by amplitude data from these 4 events. After recognizing the reality of regional influence on teleseismic amplitude measures, the LRSM amplitude data for the GNOME, SALMON, and Lake Superior explosions become more understandable and interpretable relative to NTS data (see Page 31).

As shown in Figure 17, there appears to be a strong regional correlation between amplitude of teleseismic P signal and amplitude of one second microseisms, these microseisms being composed primarily of propagating Rayleigh waves. Previous explanations for low amplitude microseisms in the WUS between the Rocky Mountains and the Sierra Nevada were based largely on assuming reflection of propagating waves when incident against the abrupt velocity changes associated with these boundaries. Such an explanation would not, of course, explain the low teleseismic P amplitudes. It would appear that the proper explanation of low Rayleigh wave amplitudes must also explain the low teleseismic P amplitudes and the explanation which immediately suggests itself is a region of abnormally low Q at comparatively shallow depth in WUS. This low Q region must be of regional extent and is no doubt related to the conditions of abnormally high heat flow in WUS.

ESTIMATION OF EVENT MAGNITUDE

The influence of local and regional geology upon recorded P signals appears to be so gross that they can greatly influence the determined magnitude of an event. It is obvious that, as soon as station calibration factors are applied to amplitude data, magnitude becomes a calibrated quantity. The relative values of the station calibration factors are fixed but their absolute values must be set on some calibration scheme.

Therefore, it should be pointed out that, due to the probable reciprocity of source and receiving stations as regards the influence of geological factors on teleseismic amplitude measurements, source correction factors must also be applied if directly comparable magnitude estimates for events occurring in all regions are to be made. One must decide upon a standard propagation path and then calibrate other measurements against the standard path. We will choose as the standard teleseismic path one having a WUS-type source or recording area and an EUS-type recording or source area. This is done because most data of relevance in detailed considerations of magnitude estimates are of this type. Thus, NTS explosions recorded at teleseismic distances in the EUS are of this type, as is SALMON recorded in WUS, GNOME recorded in WUS, and Lake Superior explosions recorded in WUS. Such path calibration is required if all magnitudes are to be related to the energy released at the source.

In addition to specifying the standard path, one must also specify the magnitude of a standard event. The amplitude correction factors given in Table 21 are such as to give the explosion MISSISSIPPI a magnitude of 4 3/4. This is essentially the magnitude obtained for MISSISSIPPI by averaging all LRSM teleseismic station values obtained in EUS. Presently employed yield versus magnitude curves are based on MISSISSIPPI having such a magnitude. The correction factors such as those of Table 21 would be applied as follows: Apply the factors to measured amplitudes. The correct calibrated magnitude is obtained by averaging these adjusted magnitude values if the source was in a WUS-type area. If the source was in a EUS-type area, a correction factor must be applied to obtain a calibrated magnitude relevant to the standard path. If an event in thick sediments in EUS is recorded teleseismically at several stations of WUS-type, one can obtain a correct calibrated value of

magnitude for averaging the magnitude values obtained at the WUS-type stations without applying either source or station calibration. Thus, for SALMON, the magnitude obtained by simply averaging the magnitude estimates at several WUS stations at teleseismic distances is 4.0. This should be essentially the correct calibrated magnitude for SALMON. If one went through the routine of applying correction factors and then converting to WUS-type source for standard path calibration, one would add 0.3 of a magnitude for WUS station corrections and subtract 0.3 of a magnitude because of the EUS-type source in thick sediments and obtain again a standard calibrated magnitude for SALMON of 4.0.

An item of some interest is that this improved understanding of the relation between source area, recording area, and determined magnitude makes it clear that previous estimates of the magnitudes of GNOME and SALMON were in error in the sense that the values used could not be legitimately related to magnitude values determined for NTS events. Again, it must be stressed that the major use of magnitude values today is in the determination of source energy rather than of mean amplitude of signal recorded. Therefore, what is desired is the magnitude of SALMON and GNOME as if they had been exploded in salt at NTS and recorded in the EUS at teleseismic distances. The calibration scheme described above will yield the appropriate magnitudes. If this procedure is followed, it is determined that the proper calibrated magnitude for SALMON is 4.0 and that for GNOME is 3.9. Thus, the oft-noted apparent anomaly that GNOME (Y = 3 kt) had a higher magnitude than SALMON (Y = 5 kt) is explained to be the result of the pattern of station distribution relative to the source and a failure to properly interpret the amplitude data rather than to any anomaly in the fraction of energy coupled from the explosion devices into the salt. These properly calibrated

magnitudes for GNOME and SALMON indicate that explosions in salt do not couple a greater fraction of energy into the ground than do explosions in granite. In fact, the SALMON and GNOME calibrated magnitude values are distinctly below those for explosions of equivalent yield in granite.

A final discussion required is another possible significance of the high amplitude signals recorded in EUS. Figure 20 indicates the situation clearly. Thus, SALMON, a 5 kt event which is exploded in WUS would have had a recorded amplitude of the P_n phase at 1000 kilometers distance of 4 mμ (at 1 second period), actually had at the same distance range an amplitude of 60 mμ. Much of this increase, of course, has previously been explained in Evernden, 1967. However, in that document failure to appreciate the factors discussed above led to averaging all magnitude values computed in that report and thus obtaining magnitudes of SALMON and GNOME several tenths too high. Without detailed amplitude and magnitude calibration such as here-in discussed, very large discrepancies in yield versus magnitude estimates can be made.

The true significance of these magnitude discrepancies as they influence the proper design of a teleseismic surveillance system must be kept clearly in mind. They do not alter the fact that stations located in WUS-type areas have lower detection thresholds than do stations in EUS-type areas. Figure 16 shows that the signal-to-noise ratio improves as mean noise level drops and, therefore, that quiet stations are the most capable, i.e., they have the lowest detection thresholds. The greater amplitude recorded in EUS-type areas results only in higher amplitude for those events detected but does not result in lower detection thresholds. A network designed for teleseismic surveillance should locate stations in the quietest sites possible and the yield

versus magnitude curves employed might as well be related to the amplitude measurements at these stations.

However, the high amplitudes observed at regional and near-regional distances for events exploded and recorded in EUS-type areas are so high that they markedly affect previous conclusions as to the significance and utility of such stations as regards their capability to detect the P_n phase of small yield devices (SALMON, a 5 kt device gave signals of 60 mμ at 1000 kilometers range in EUS).

B-FACTOR CURVE

The analysis leading to individual station amplitude correction factors also yielded a curve of variation of amplitude as a function of distance. Table 22 indicates the values determined when using All data uncorrected for station factors, All data corrected for station factors, Northwest data corrected for station factors, and South data corrected for station factors. Numbers in parentheses after the values indicate the standard deviation of residuals. For All data (corrected) and Northwest data, the values on the 13.2, 14.5, and 16.3 legs are positive, implying increase of amplitude with increasing epicentral distance. Amplitudes on the 12.4 leg decrease rapidly with increasing distance as do amplitudes on the 24.5 leg. Positive values are obtained with South data on the 13.2 and 16.3 legs, data on the 14.5 leg yielding a negative value.

By use of data for earthquakes recorded on adjacent legs, a complete B-factor curve can be generated. It is, of course, actually derived in terms of log A/T with no established calibration relative to a magnitude scale. Thus, Table 23 indicates the derived pattern of log A/T as a function of

distance, assuming a value of log A/T of 3.00 at 2700 kilometers. The values used in Table 23 are those for All data (corrected) while the log A/T of this table is plotted on Figure 21, in conjunction with Gutenberg's B-factor curve and a recently published curve generated by Clawson of Geotech by use of explosion data. The placement of the log A/T curve of this report relative to Gutenberg's B-factor curve is arbitrary and two positions of our curve are shown as Position A and Position B. Position A was selected so that our log A/T curve agreed on the average with Gutenberg's curve in the distance range 7000 - 11000 kilometers. The agreement of shapes of our curve and Gutenberg's curve in this region are astonishing. His indicates increase of amplitude from 6800 kilometers to 8800 kilometers, followed by a high rate of decrease of amplitude at greater distances. This character is essentially exactly reproduced by the log A/T curve of this report. In the distance range 3000 to 6000 kilometers, the detailed shape of our log A/T curve is again in remarkable agreement with the shape of Gutenberg's, with amplitudes in the distance range 3800 - 5000 kilometers being markedly greater than at shorter or longer distances.

There is, however, a major discrepancy between the B-factor curve of Gutenberg and that of this report. Though the two curves agree in detailed shape in the distance ranges 7000 - 11000 kilometers and 3000 - 5000 kilometers, they considerably disagree in the distance range 5000 - 7000 kilometers. If the two curves are adjusted to yield the same magnitude at short teleseismic distances, they will show a discrepancy of 0.3 magnitude at long teleseismic

distances. The data of this report might suggest that Gutenberg's curve is miscalibrated between short teleseismic and long teleseismic distances. In this regard, 70 Eurasian earthquakes recorded at a set of quiet stations were investigated to see whether, when using his curve, there was a systematic discrepancy between magnitude estimates at short and long teleseismic distances. Seventy-two percent of the events had higher computed magnitudes at long teleseismic distances (8000 - 11000 kilometers) than they did at short teleseismic distances (3000 - 5000 kilometers), the average difference being 0.3 magnitude. The remaining 28% were equally split between events showing no discrepancies and events showing lower computed magnitudes at long teleseismic distances. An approximate 0.2 magnitude differential appeared to be present in the total body of data. This investigation would suggest that Gutenberg's curve is miscalibrated and that magnitudes as determined by it are generally too high at long teleseismic distances by 0.2 - 0.3 magnitude units.

The question remains as to how the log A/T curve of this report should be converted to a B-factor curve. If the criterion were to achieve agreement with Gutenberg's at long teleseismic distances, curve A of Figure 21 would be employed. If the relevant criterion, however, were to agree with his at short teleseismic distances, curve B would be employed. The latter seems to us the more logical approach, particularly in light of the fact that amplitudes in this distance range have been used previously to calibrate curves at regional and near-regional distances and to establish magnitudes of NTS explosions and then to determine yield versus magnitude relationships. Thus, we would suggest that the curve through the B segments in Figure 21 is the best now available for intercalibrating observational earthquake data at all

teleseismic distances. The one published by Clawson is not sufficiently expressive of the detailed variations in amplitude that do exist in earthquake observations. Clawson's curve indicates, even in its too generalized form, a greater decrease of amplitude with distance from short or long teleseismic distances than does the one in this report. Since Clawson's curve is entirely based on explosion data, this discrepancy may be the result of the high frequency content of explosion signals and the attenuation of high frequency components at long teleseismic distance.

The final major interest of the log A/T versus Δ curve of Figure 21 is its relationship to the travel-time curve previously derived, and the evidence Figure 21 gives for or against the near-segmented character of the P travel-time curve. The marked change in slope of the amplitude curve between the 12 and 13 legs (-2.5 on the 12.5 leg and +1.7 on 13.2 leg), as well as the .15 magnitude discrepancy, seems to imply the reality of the near-segmented nature of the travel-time curve, i.e., of the existence of a narrow region in the mantle displaying high rate of velocity change with depth.

The 0.3 magnitude discrepancy between the 13.2 and 14.5 legs, a phenomenon clearly shown in Gutenberg's data, also supports the existence of a zone of rapid velocity change. Variations in slope and amplitude between the 14.2, 16.3, 18.0, and 19.6 legs are not as large. However, the reversal in curvature between the 16.3 and 18.0 legs was indicated in Gutenberg's data and, in association with the .15 magnitude increase in amplitude, strongly suggests a localized source in the mantle. The discrepancy in amplitude between the 19.6 and 22.0 legs (.25 magnitude) and the marked difference in rate of decrease of amplitude with distance seem also to

suggest the reality of a zone of high rate of change of velocity in the lower mantle. The change in slope (-4.6 to -12.3) between the 22 and 25 legs is also suggestive of the same phenomenon. The differential in amplitudes, however, is so small that it cannot be used as support for this interpretation. In general, it would appear that the amplitude data here obtained do support the concept of a nearly segmented travel-time curve such as that of Figure 11. The reasonable conclusion to draw from such a velocity structure is that the zones of rapid velocity change are associated with phase transitions in the mantle. Such a hypothesis would permit large scale convection while one based on such velocity transitions being related to compositional changes in the mantle would probably bar the possibility of convection.

TABLE I

Events Used in Travel-Time Curve Study

	No.	Date	Lat	Long	Depth (km)	Time	Location
	1A	13 Sep 63	37.061 N	116.032 W	0	17:00:00.1	BILBY - NTS
	1B	23 Jul 65	37.090 N	116.033 W	0	17:00:00.0	ROCKEN - NTS
	1C	20 Feb 64	37.151 N	116.040 W	0	15:30:00.1	FLYCHIEFET - NTS
	1D	27 Jun 62	37.043 N	116.035 W	0	16:00:00.1	HAYMAKER - NTS
	1E	03 Mar 65	37.064 N	116.037 W	0	19:13:00.0	WHOTAIL - NTS
	1F	24 Apr 64	37.150 N	116.055 W	0	20:10:00.2	TUBP - NTS
	1G	15 Jul 65	37.197 N	74.352 W	900'	14:16:00.1	CHASE III - Atlantic
	1I	17 Sep 64	30.017 N	72.242 W	4000'-5000'	22:07:45.0	CHASE II - Atlantic
NV	1	13 Oct 63	45:05:06 N	149:27:48 E	(62)	05:17:59.1	Kurils
	2	10 Aug 63	50:24:54 N	177:00:12 W	16	18:43:13.7	Aleutians
	3	26 Oct 63	44:44:12 N	149:58:30 E	24	05:59:42.7	Kurils
	4	11 Dec 63	51:11:48 N	179:16:36 W	70	17:00:17.0	Andreanof Islands
	5	08 Aug 63	54:13:38 N	168:12:30 E	113	02:15:03.6	Near Islands
	6	09 Dec 63	54:45:00 N	159:40:48 W	28	05:30:27.3	Alaska Peninsula
	7	01 Feb 64	51:45:24 N	170:59:42 W	45	01:47:53.4	Fox Island
	8	07 May 64	30:37:48 N	137:30:12 E	583	11:11:07.7	Honshu
	9	09 Dec 64	27:21:36.5 S	63:18:30 W	593	13:35:44.4	Brazil
	11	18 Jun 63	28:47:54 N	130:04:36 E	46	04:02:36.5	Ryukyu
	12	28 Nov 63	52:19:54 N	174:02:30 E	53	15:13:13.9	Near Island
	13	06 Jan 64	50:52:18 N	157:16:06 E	86	23:45:29.2	Kamchatka
	14	08 Feb 64	52:13:24 N	175:30:00 E	94	11:17:48.5	Rat Island
	15	09 May 64	52:00:18 N	169:35:48 W	29	02:02:29.7	Andreanof Islands
	16	17 Aug 63	30:49:06 N	131:00:54 E	38	11:12:42.3	Ryukyu Islands
	17	06 Jan 64	27:16:36 N	127:26:36 E	131	08:54:45.3	Ryukyu Islands
	20	18 Mar 64	52:33:00 N	153:40:12 E	440	04:37:27.1	Sea of Okhotsk
	22	15 Aug 63	13:43:42 S	69:18:00 W	563	17:25:00.5	Peru-Bolivia
	23	12 Oct 63	44:43:22.0 N	149:09:43.2 E	34	11:26:57.5	Kurils
	24	18 Jan 64	18:41:36 N	69:21:12 W	121	22:36:19.7	Dominican Republic
	25	03 Aug 63	07:23:30 N	36:40:42 W	(0)	10:21:29.7	Atlantic
	26	24 Jun 63	59:26:06 N	152:02:18 W	45	04:26:36.9	Prince William Sound
	27	28 Mar 64	56:23:54 N	154:00:24 W	81	12:20:56	Alaska
	28	28 Mar 64	56:23:36 N	152:05:48 W	44	09:01:03.4	Alaska
	29	28 Mar 64	59:43:54 N	148:40:24 W	27	20:29:07.0	Alaska
	30	30 Jun 64	46:32:24 N	144:30:24 E	364	20:00:26.7	Sea of Okhotsk
	31	29 Dec 63	18:16:12 S	69:16:48 W	125	17:15:40.0	Bolivia
	32	17 Jun 63	60:25:30 N	149:51:36 W	16	18:32:12.4	Tyhon
	33	31 Mar 64	50:47:48 N	130:09:54 W	15	09:01:31.2	Vancouver
	34	30 Mar 64	56:37:24 N	152:49:24 W	20	02:18:06.4	Prince William Sound
	35	12 Jan 64	53.2 N	166.3 W	33	06:00:15.2	Fox Islands
	36	23 Mar 64	61.1 N	147.8 W	0	03:36:10.0	Alaska
	38	16 Nov 64	49:48:36 N	78:08:24 E	0	06:06:00.0	Semipalatinsk
	40	25 Oct 64	73:23:24 N	54:22:12 E	0	08:00:00.6	Novaya Zemlya
	41	16 Nov 63	44.3 N	149.0 E	50	02:30:07.0	Kuril Islands
	42-49	unassigned					
	50	16 Mar 64	44:46:36 N	147:02:18 E	148	06:44:34.1	Kuril Islands
	52	04 Aug 64	46:35:24 N	151:20:48 E	101	17:24:30.4	Kuril Islands
	53	26 Jan 64	16:14:48 S	71:29:30 W	116	09:09:36.3	Peru
	55	03 Feb 63	07:48:00 N	35:54:00 W	33	10:34:25.7	Atlantic
	56	17 Sep 64	44:30:42 N	31:16:42 W	24	15:02:02.3	Atlantic
	57	21 Jun 64	51:00:00 N	157:00:00 E	51	01:33:11.2	Kamchatka
	58	24 Mar 63	51:43:48 N	178:13:30 W	57	23:35:24.4	Andreanof Islands
	59	26 Sep 64	50:10:10 N	176:50:12 W	33	05:20:07.3	Andreanof Islands
	60	17 Sep 63	10:37:42 S	78:02:00 W	61	05:54:33.7	Central Peru
	61	14 Jul 64	53:15:54 N	159:39:12 E	40	13:40:28.7	Kamchatka
	62	22 Mar 64	05:34:42 S	76:56:18 W	147	07:45:41.3	Northern Peru
	63	22 Mar 64	53:56:24 N	160:26:00 E	30	00:52:38.9	Kamchatka
	64	06 Feb 64	06:43:18 N	73:13:30 W	140	04:35:56.8	Columbia
	65	22 Aug 63	04:09:18 N	76:16:36 W	100	23:20:20.8	Columbia
	66	23 Oct 63	19:20:30 N	155:27:30 W	5	20:24:06.1	Hawaii
	67	23 Sep 63	51:18:00 N	179:12:00 W	33	17:02:36.6	Andreanof Islan'
	70	23 Oct 63	41:14:54 N	144:18:36 E	50	09:47:11.0	Honshu
	71	03 Dec 63	22:24:00 S	69:18:0 W	18	23:03:41.6	Chile
	72	07 May 64	40:33:12 N	139:04:00 E	33	20:13:49.7	Honshu
	73	07 May 64	40:32:30 N	138:59:12 E	33	07:58:16.3	Honshu
	74	05 Oct 63	16:01:24 S	173:02:06 W	79	01:55:37.5	Tonga Islands
	75	03 Oct 63	32:07:07 N	131:43:24 E	33	23:24:34.1	Kyushu
	76	24 Jan 64	38:42:00 N	129:24:00 E	542	17:17:45.5	Korea
	77	15 Jan 64	29:03:30 N	140:55:18 E	70	21:36:07.3	Honshu
	78	06 Apr 64	41:49:30 S	83:50:24 W	33	11:18:41.2	Chile
	80	01 May 62	24:03:36 N	05:02:24 E	0	10:00:00.5	Algeria
	82	22 Apr 64	59:06:00 N	34:54:00 W	90	09:46:54.2	North Atlantic
	83	16 Mar 64	36:[illegible]:00 N	95:30:00 E	33	01:05:17.6	China
	84	17 Sep 63	10:[illegible]:00 S	165:18:00 E	17	19:20:00.2	Santa Cruz
	85	17 Aug 63	17:43:[illegible].6 N	94:07:37.2 W	174	11:34:26.5	Mexico

TABLE 2

Location and Geology of LRSN Sites

Location	Noise Level (50% nu)	Lat (N)	Long (N)	Elevation	Geology
AS-TX	20 - 25	35°25'48"	101°55'50"	3240'	Permian-claystone, dolomite (Blain Permian Formation.)
BL-WV	25 - 30	37 47 56	81 18 36	2000	Pottsville Formation (Pennsylvania) sandstone
BR-PA	11	39 55 27	78 50 41	2180	Catskill Formation (Upper Devonian) sandstone
BX-UT	2 - 3	37 33 48	109 26 05	5600	Morrison Formation (Jurassic) - Salt Wash sandstone
CP-CL	6 - 7	32 43 44	116 22 16	3900	LaPosta Formation (Jurassic) Quartz diorite
CU-WV	9 - 10	38 40 38	115 27 18	5400	Pogonip Formation (Ordovician) limestone
DH-NY	35 - 40	42 14 39	74 53 18	2140	Catskill Formation (Devonian) sandstone
DR-CO	2 - 3	37 27 53	107 47 00	7300	Pre-Cambrian granite
DU-OK	8 - 9	34 02 11	96 13 04	650	Bokchito Formation (Cretaceous) 700' of Cretaceous on basement (Pre-Cambrian granites to Carboniferous)
EB-MT	5 - 6	49 37 40	95 37 20	1025	Pre-Cambrian granite
ER-WV	2 - 5	39 12 32	115 42 37	6400	White Pine Shale (Pennsylvania) 10,300' deep well still in Ordovician - mostly limestone
FR-MA	50 - 55	46 06 00	106 26 25	2700	Fort Union Formation (Paleocene) Basement depth?
GI-MA	20 - 25	47 11 34	104 13 10	2400	Fort Union Formation (Paleocene) Basement depth?
HN-ND	30 - 35	48 56 53	98 41 33	1600	Pierre Shale (Cretaceous) 3000' to Basement
HL-ID	1 - 6	43 38 50	114 15 02	6200	Carboniferous - meta limestone - southeast flank of Idaho Batholith
HN-NE	20 - 21	46 09 43	67 59 09	700	Silurian, Dense, siliceous slate - vertical
HN-UT	2 - 3	37 01 22	112 49 39	5700	Navajo Formation (Jurassic) sandstone - 40[illegible]' to Paleozoic, 5000' further to Pre-Cambrian
LC-NM	2 - 3	32 24 08	106 35 58	5200	Magdalena Formation (Pennsylvania) limestone
LS-NH	20 - 25	44 14 18	71 55 21	940	Metamorphosed Littleton Formation (Devonian)
MN-WV	4 - 5	38 26 10	118 08 53	5000	Massive limestone and metamorphic rocks-intruded by igneous bodies.
MV-CL	7 - 8	39 12 47	121 17 35	600	Mudflow and gravels overlying Jurassic basic, meta-igneous, volcanic rocks
RR-ON	5 - 6	50 50 20	93 40 20	1200	Pre-Cambrian granite
RT-NM	7 - 8	36 43 46	104 21 37	6400	Niobrara Formation (Cretaceous) limestone and shale
RY-ND	25 - 30	48 05 50	101 29 40	2100	Glacial drift (Pleistocene) 100'-150' to Eocene-9000' further to basement
SR-TX	9 - 10	35 04 58	100 21 50	2200	Blaine Formation (Permian)
WI-WV	2 - 3	41 21 02	117 27 30	5000	Limestone and metamorphic (Triassic)

TABLE 3

Station Time Anomalies
(Elevation Effect Removed)

Station	Time Anomaly (seconds)
AZ-TX	-.43
BL-WV	-.19
BR-PA	.05
BX-UT	-.50
CP-CL	-.29
CU-NV	.16
DH-NY	-.10
DR-CO	-.02
DU-OK	-.77
ED-MT	-.85
EK-NV	.12
FR-MA	-.20
GI-MA	.31
GV-TX	-.06
HR-ND	-.39
HL-ID	-.03
HN-ME	.03
KN-UT	.29
LC-MM	-.06
LS-NH	.44
MN-NV	.06
MV-CL	-.39
RK-ON	-1.07
RT-NM	-.17
RY-ND	.20
SK-TX	-.36
WI-NV	.23

TABLE 4

Coefficients of Travel-Time Curve - All Data

A - Equation: $t = a + b\Delta$

Leg Designation	b	σ
10.4	.09634	.573
12.5	.08031	.345
13.4	.07459	.429
14.5	.06880	.353
16.3	.06140	.401
18.2	.05488	.340
19.5	.05133	.315
22.0	.04541	.283
24.2	.04127	.431

B - Equation: $t = a + b\Delta + c\Delta^2$

Leg Designation	b	c	σ
10.4	.09483	$+ 3.337 \times 10^{-7}$	.573
12.5	.09205	-17.987	.332
13.4	.10315	-32.742	.372
14.5	.07167	- 2.728	.352
16.3	.09820	-27.563	.344
18.2	.10954	-35.162	.307
19.5	.03407	+10.117	.315
22.0	.08132	-19.157	.263
24.2	.02776	+ 6.344	.423

C - Equation: $t = a + b\Delta + d\Delta^3$

Leg Designation	b	d	σ
10.4	.09493	$+ 9.039 \times 10^{-11}$	.573
12.5	.08614	-18.819	.332
13.4	.08895	-25.103	.372
14.5	.07032	- 1.711	.352
16.3	.07977	-13.722	.344
18.2	.08226	-15.100	.307
19.5	.04300	+ 3.813	.315
22.0	.06339	- 6.818	.263
24.2	.03441	+ 2.013	.423

TABLE 5

Coefficients of Travel-Time Curve
Northwest Data

A - Equation: $t = a + b\Delta$

Leg Designation	b	σ
12.5	.08052	.331
13.4	.07446	.438
14.5	.06952	.298
16.3	.06157	.419
18.2	.05392	.392
19.5	.05145	.283
22.0	.04537	.267
24.2	.04062	.296

B - Equation: $t = a + b\Delta + c\Delta^2$

Leg Designation	b	c	σ
12.5	.08858	-12.302×10^{-7}	.323
13.4	.11039	-41.076	.331
14.5	.07144	- 1.763	.297
16.3	.11055	-36.711	.289
18.2	.09427	-25.448	.297
19.5	-.07140	+72.053	.259
22.0	.07784	-17.286	.250
24.2	.07192	-14.857	.263

TABLE 6

Coefficients of Travel-Time Curve
South Data

A - Equation: $t = a + b\Delta$

Leg Designation	b	σ
12.5	.08072	.368
13.4	.07504	.407
14.5	.06787	.350
16.3	.06125	.416
18.2	.05558	.345
19.5	.05126	.421
22.0	.04677	.274

B - Equation: $t = a + b\Delta + c\Delta^2$

Leg Designation	b	c	σ
12.5	.09386	-20.002×10^{-7}	.346
13.4	.05519	+23.056	.388
14.5	.06079	- 6.471	.348
16.3	.09011	-21.606	.384
18.2	.06784	-20.875	.340
19.5	.16775	-68.109	.397
22.0	.09392	-25.918	.177

TABLE 7

Coefficients of Travel-Time Curve

All data - Two legs simultaneously

A - Equation: $t = a + b\Delta + c\Delta^2$

Leg Designation	b	c	σ	(σ_{-1}/σ_2) (Table 4)
12.5/13.4	.09762	-26.129×10^{-7}	.354	.354/.429
13.4/14.5	.09636	-25.526	.488	.429/.353
14.5/16.3	.10118	-29.889	.434	.353/.401
16.3/18.2	.10259	-30.772	.387	.401/.340
18.2/19.5	.08967	-22.612	.463	.340/.315
19.5/22.0	.10786	-33.371	.357	.315/.283
22.0/24.2	.08617	-18.693	.449	.283/.431

B - Equation: $t = a + b\Delta + c\Delta^3$

Leg Designation	b	d	σ
12.5/13.4	.08768	-22.590×10^{-11}	.349
13.4/14.5	.08398	-17.411	.490
14.5/16.3	.08318	-16.445	.432
16.3/18.2	.08069	-14.354	.383
18.2/19.5	.07139	- 9.308	.464
19.5/22.0	.07777	-12.320	.358
22.0/24.2	.06143	- 6.209	.453

TABLE 8

Analysis of Variance

Leg Designation	Comparison	F	1' 2	P
12.5	All $(a + b\Delta)$ vs All $(a + b\Delta + c\Delta^2)$	3.44	1,43	.05-.10
	All $(a + b\Delta + c\Delta^2)$ vs E $(a + b\Delta)$*	3.15	13,29	.005
	E $(a + b\Delta)$ vs E $(a + b\Delta + c\Delta^2)$*	2.52	7,14	.05-.10
13.4	All $(a + b\Delta)$ vs All $(a + b\Delta + c\Delta^2)$*	22.44	1,68	.005
	All $(a + b\Delta) + c\Delta^2)$ vs E $(a + b\Delta)$	.67	114,53	High
	All $(a + b\Delta + c\Delta^2)$ vs E $(a + b\Delta + c\Delta^2)$*	1.46	18,37	.15
	All $(a + b\Delta)$ vs E $(a + b\Delta)$*	2.01	15,53	.03-.05
14.5	All $(a + b\Delta)$ vs All $(a + b\Delta + c\Delta^2)$	.5	1,95	High
	All $(a + b\Delta)$ vs E $(a + b\Delta)$*	2.99	17,79	.005
	E $(a + b\Delta)$ vs E $(a + b\Delta + c\Delta^2)$	.2	14,61	High
16.3	All $(a + b\Delta)$ vs All $(a + b\Delta + c\Delta^2)$*	31.07	1,85	.005
	All $(a + b\Delta + c\Delta^2)$ + E $(a + b\Delta + c\Delta^2)$	.80	22,62	High
18.2	All $(a + b\Delta)$ vs All $(a + b\Delta + c\Delta^2)$*	22.65	1,120	.005
	All $(a + b\Delta + c\Delta^2)$ vs E $(a + b\Delta)$	1.06	16,83	.40
	All $(a + b\Delta + c\Delta^2)$ vs E $(a + b\Delta + c\Delta^2)$*	1.99	30,60	.01
19.5	All $(a + b\Delta)$ vs E $(a + b\Delta + c\Delta^2)$*	1.50	25,30	.15
22.0	All $(a + b\Delta)$ vs All $(a + b\Delta + c\Delta^2)$*	17.37	1,110	.005
	All $(a + b\Delta)$ vs E $(a + b\Delta)$*	2.13	20,90	.01
	All $(a + b\Delta) + c\Delta^2)$ + E $(a + b\Delta + c\Delta^2)$*	1.38	30,66	.15
	All $(a + b\Delta)$ vs E $(a + b\Delta + c\Delta^2)$*	1.88	30,66	.01-.02
24.2	E' $(a + b\Delta)$ vs E' $(a + b\Delta + c\Delta^2)$	1.60	10,24	.15
	All' $(a + b\Delta)$ vs All' $(a + b\Delta + c\Delta^2)$*	2.81	1,53	.05-.10
	All' $(a + b\Delta + c\Delta^2)$ vs E' $(a + b\Delta + c\Delta^2)$	2.95	14,30	.01

"E" means each event analyzed separately, each event having independently estimated values of a, b, c, or d.

"All" means all data on each leg handled together, yielding one value of b, c, or d, and an a value for each event.

TABLE 9

Standard Deviation/Residuals

Leg	Event	No. Of Stations	All Events ($a + b\Delta$)	All Events ($a + b\Delta + c\Delta^2$)	All Events ($a + b\Delta + d\Delta^3$)	Each Event ($a + b\Delta$)	Each Event ($a + b\Delta + c\Delta^2$)
12.5	--	66	.345	.332	.332		
	06	5				.121	.103
	24	4				.177	.115
	27	5				.140	.111
	29	8				.277	.214
	32	4				.348	.095
	34	5				.373	.164
	85W	4				.221	.017
13.4	--	89	.429	.372	.372		
	02	4				.169	.131
	06	10				.317	.225
	16	5				.245	.245
	24	8				.327	.327
	27	4				.085	.082
	35	13				.411	.353
	64	6				.326	.256
	65	5				.520	.486
	66	7				.310	.265
	82	5				.661	.284
14.5	--	121	.353	.352	.352		
	02	10				.235	.213
	04	8				.172	.122
	05	5				.078	.067
	07	4				.131	.085
	12	7				.303	.281
	14	10				.232	.220
	55	4				.058	.034
	59	10				.412	.395
	60	9				.377	.377

TABLE 9 (Cont'd.)

Standard Deviation/Residuals

Leg	Event	No. Of Stations	All Events ($a + b\Delta$)	All Events ($a + b\Delta + c\Delta^2$)	All Events ($a + b\Delta + d\Delta^3$)	Each Event ($a + b\Delta$)	Each Event ($a + b\Delta + c\Delta^2$)
	62	6				.434	.428
	64	10				.175	.170
	65	9				.345	.252
	66	5				.299	.233
	67	6				.251	.251
16.0	--	113	.402	.344	.344		
	05	5				.359	.287
	12	4				.121	.008
	13	13				.373	.302
	22	6				.597	.460
	31	9				.385	.385
	53	10				.188	.187
	56	4				.385	.358
	57	8				.366	.334
	60	16				.454	.390
	61	7				.465	.071
	62	7				.266	.265
	63	9				.457	.181
18.0	--	122	.340	.307	.307		
	01	10				.283	.242
	03	8				.443	.271
	23	10				.329	.287
	25	6				.157	.151
	30	8				.223	.220
	31	7				.195	.189
	40	6				.262	.255
	41	8				.256	.146
	50	9				.249	.203

TABLE 9 (Cont'd.)

Standard Deviation/Residuals

Leg	Event	No. Of Stations	All Events ($a + b\Delta$)	All Events ($a + b\Delta + c\Delta^2$)	All Events ($a + b\Delta + d\Delta^3$)	Each Event ($a + b\Delta$)	Each Event ($a + b\Delta + c\Delta^2$)
	51	4				.089	.086
	52	7				.288	.145
	53	6				.325	.260
	55	5				.191	.190
	63	5				.148	.075
	70	8				.279	.274
	71	6				.374	.303
19.6	--	85	.315	.315	.315		
	01	4				.302	.036
	03	4				.132	.131
	13	5				.177	.062
	20	6				.427	.286
	23	4				.136	
	25	4				.433	.091
	55	5				.365	.098
	57	4				.131	.035
	70	6				.195	.194
	71	11				.404	.364
72	72	8				.269	.245
	73	8				.261	.160
	74	4				.088	.087
22.0	--	137	.283	.263	.263		
	01	4				.151	.084
	03	7				.308	.257
	08	10				.187	.178
	18	7				.216	.202
	23	6				.231	.197
	30	7				.255	.255

TABLE 9 (Cont'd.)

Standard Deviation/Residuals

Leg	Event	No. Of Stations	All Events ($a + b\Delta$)	All Events ($a + b\Delta + c\Delta^2$)	All Events ($a + b\Delta + d\Delta^3$)	Each Event ($a + b\Delta$)	Each Event ($a + b\Delta + c\Delta^2$)
	50	7				.099	.070
	52	5				.188	.188
	74	9				.288	.277
	75	9				.267	.228
	76	12				.260	.255
	77	12				.236	.165
	78	4				.107	.105
	84	4				.158	.154
25.0	--	78	.431	.423	.423		
	38	6				.567	.321
	72	6				.200	.150
	73	7				.190	.184
	77	5				.246	.203
	78	5				.154	.142
	80	4				.685	.567
	83	10				.219	.207
	84	9				.275	.156

TABLE 10

Travel-Time Curve Parameters

Log	Event	No of Stations	Depth (km)	Lat	Long	Distance Range	Legvise $a + b\Delta$ a	b	$a + b\Delta + c\Delta^2$ a	b	c	Eventwise $a + b\Delta$ a	b	$a + b\Delta + c\Delta^2$ a	b	c
12.2								.080301		.094049	-1.7987(-06)					
	06	5	28	55N	160 W	3335-3687	100.2		81.2			102.5	.079653	164.9	.044084	5.0484(-06)
	24	4	121	19N	69 W	3146-3688	91.5		72.5			95.8	.079032	163.4	.039095	5.8726(-06)
	27	5	81	56N	154 W	3305-3611	94.5		75.4			94.9	.080191	-5.0	.137941	-8.3490(-06)
	29	8	27	60N	149 W	3157-3595	100.6		81.5			105.4	.078851	229.4	.005289	1.0887(-05)
	32	4	16	60N	141 W	2658-3272	101.5		82.5			99.5	.080943	36.6	.123035	-6.6499(-06)
	34	5	20	57N	153 W	3247-3652	100.5		81.4			90.6	.083203	150.7	.22289	-2.8177(-05)
	35W	4	174	18N	94 W	2856-3572	60.1		41.1			58.6	.080803	99.7	.055248	3.9456(-06)
13.4								.074593		.10315	-3.274(-06)					
	02	4	16	50N	177 W	4470-4751	123.7		61.7			133.3	.072511	416.4	-.050364	1.3325(-05)
	06	10	28	55N	160 W	3998-4800	122.0		60.1			122.2	.074554	52.8	.105953	-3.5356(-06)
	16	5	29	52N	170 W	4214-4715	122.7		60.6			140.4	.070647	140.6	.070566	9.0667(-09)
	24	8	131	18N	69 W	3944-4675	113.1		51.1			108.8	.075606	105.8	.076975	-1.5927(-07)*
	27	4	81	56N	154 W	3913-4492	116.5		54.6			105.7	.077186	117.7	.071483	6.7876(-07)
	35	13	33	53N	166 W	3905-4758	111.8		59.8			122.7	.074384	60.8	.103027	-3.2972(-06)*
	64	6	140	07N	73 W	3929-4878	112.2		50.2			110.5	.074998	194.6	.035441	4.6416(-06)*
	65	5	100	04N	76 W	3951-4864	116.3		54.2			117.1	.074269	233.2	.020755	6.1716(-06)*
	66	7	5	19N	155 W	3945-4878	126.3		64.3			127.2	.074402	71.1	.100422	-3.0106(-06)*
	82	5	90	59N	35 W	4020-4789	122.5		60.5			120.9	.074961	- 72.0	.162793	-9.9585(-06)*
14.5								.068796		.0717653	-2.7275(-07)					
	02	10	16	50N	177 W	5154-5986	152.4		144.3			150.0	.069261	93.6	.09009	-1.9061(-06)*
	04	8	70	51N	179 W	5179-5620	146.1		138.0			141.3	.069700	232.8	.035252	3.2376(-06)
	05	5	113	54N	168 E	5406-5919	141.1		133.0			139.4	.069095	209.6	.044130	2.2187(-06)
	07	4	45	52N	171 W	5090-5542	148.5		140.4			145.0	.069452	515.4	-.069966	1.3099(-05)
	12	7	53	52N	174 E	5219-5803	148.1		140.1			147.3	.06892	50.0	.104214	-3.1954(-06)*
	14	10	50	52N	175 E	5131-5878	143.6		135.6			133.3	.070666	107.2	.000129	-8.5000(-07)
	55	4	33	08N	36 W	5240-5638	152.8		144.7			150.4	.069245	66.8	.10015	-2.8295(-06)
	59	10	33	50N	177 W	5139-5813	151.0		142.9			149.3	.069104	65.4	.09888	-2.8193)-06)
	60	9	61	11S	78 W	5205-5907	147.7		139.C			153.0	.067845	154.9	.0671486	6.2671(-06)*
	62	6	147	6S	77 W	5225-5790	138.9		130.8			148.2	.067098	81.4	.0913931	-2.2056(-06)*
	64	10	140	07N	73 W	5192-5717	139.4		131.3			144.3	.067805	170.1	.0583320	8.0473(-07)*
	65	9	100	04N	76 W	5184-5724	143.5		135.4			143.0	.06881	309.7	-.0213261	8.2345(-06)*
	66	5	5	19N	155 W	5019-5772	154.9		146.8			155.1	.068760	63.5	.1029037	-3.1751(-06)*
	67	6	33	51N	179 W	5051-5945	150.3		142.2			150.5	.068757	158.3	.0458219	2.7606(-07)*

TABLE 10 (Cont'd.)

Travel-Time Curve Parameters

Leg	Event	No of Stations	Depth (km)	Lat	Long	Distance Range	Legvise $a + bA$ a	Legvise $a + bA$ b	Legvise $a + bA + cA^2$ a	Legvise $a + bA + cA^2$ b	Legvise $a + bA + cA^2$ c	Downwise $a + bA$ a	Downwise $a + bA$ b	Downwise $a + bA + cA^2$ a	Downwise $a + bA + cA^2$ b	Downwise $a + bA + cA^2$ c
	01	4	(62)	45N	149 W	8321-8702	267.5		341.1			253.5	.052961	1536.7	-.266419	1.7607(-05)
	03	4	34	49N	150 W	8339-8722	270.8		344.4			255.1	.053164	180.2	.070741	-1.8310(-06)
	13	5	86	51N	157 E	8243-8657	265.9		339.5			272.9	.050509	2603.5	-.468900	2.0229(-05)
	20	6	440	53N	154 E	8346-8698	227.7		301.3			227.8	.051312	2303.3	-.412055	2.7261(-05)
	23	4	34	45N	149 E	8364-8746	271.8		345.4			275.7	.050000	10.2	.115082	-3.8798(-06)
	55	5	33	08	36 W	8331-8808	272.7		346.2			269.1	.051738	-954.9	.337695	-1.6606(-06)
	57	4	51	51N	157 W	8251-8659	270.1		343.7			266.4	.049426	1633.9	-.266313	1.0403(-06)
	70	6	50	41N	144 E	8884-8405	270.1		343.7			259.8	.052563	72.1	.006728	-2.3008(-06)
	71	11	18	22S	69 W	8292-8439	274.3		347.8			264.1	.050170	1193.5	-.163611	1.2961(-06)
	72	8	33	41N	139 E	8284-8741	272.1		345.6			275.1	.050073	681.9	-.066541	5.6663(-06)
	73	8	33	40N	139 E	8300-8757	271.5		345.0			275.2	.050005	1818.2	-.123102	1.0193(-06)
	74	6	79	16S	173 W	8311-8618	266.2		339.8			261.9	.051834	130.0	.003046	-1.0463(-06)
22.0								.045413		.001324	-1.8157(-06)					
	01	4	(62)	45N	149 E	9061-9656	320.5		152.3			317.7	.045720	95.3	.101622	-3.0002(-06)
	03	7	34	45N	150 E	9064-9653	323.3		155.1			313.8	.046416	717.3	-.030834	4.0871(-06)
	08	10	503	31N	138 E	9020-9066	274.4		106.2			281.5	.044657	161.0	.070433	-1.3779(-06)
	10	7	38	31N	131 E	8259-9048	324.2		156.1			338.2	.044364	104.2	.093575	-2.5265(-06)
	23	6	34	45N	149 E	9135-9681	324.3		156.1			317.4	.047145	-22.5	.118300	-8.8375(-06)
	30	7	47N	47N	145 E	9266-9778	287.3		119.1			293.1	.044805	138.6	.035230	5.0357(-07)
	50	7	14S	45N	147 E	9261-9795	311.4		143.2			312.2	.045336	88.2	.093383	-2.4877(-06)
	52	5	101	47N	151 E	9067-9322	317.8		148.7			330.2	.045064	234.8	.088013	-1.1225(-06)
	74	9	79	16S	173 W	8908-9785	318.7		150.6			323.6	.044081	221.8	.084007	-1.6881(-06)
	75	9	16	32N	132 E	9112-9897	324.4		156.2			321.9	.045671	17.8	.100073	-3.3971(-06)
	76	12	542	39N	129 E	9063-9754	270.4		102.2			274.0	.045030	366.0	.088076	1.3013(-06)
	77	12	70	29N	141 E	8925-9182	320.1		151.9			361.1	.045031	88.2	.086618	-3.6095(-06)
	78	4	70	42S	84 W	8951-9182	325.2		157.0			321.2	.045039	279.8	.086082	-4.9178(-07)
	84	4	17	10S	165 E	9313-9782	326.6		158.4			329.9	.045066	214.1	.089329	-1.3782(-06)
25.0								.041272		.006216	-1. 00(-06)					

TABLE 10 (Cont'd.)

Travel-Time Curve Parameters

Leg	Event	No of Stations	Depth (km)	Lat	Long	Distance Range	Legwise $a + b\Delta$ a	Legwise b b	Legwise $a + b\Delta + c\Delta^2$ a	Legwise b b	Legwise c c	Eventwise $a + b\Delta$ a	Eventwise b b	Eventwise $a + b\Delta + c\Delta^2$ a	Eventwise b b	Eventwise c c
	36	6	0	50N	78 E	10108-10902	368.9		259.9			368.0	.061362	398.3	.185435	-6.8564(-06)
	72	6	33	41N	139 E	10054-10427	365.3		256.3			353.7	.062404	641.8	.237026	-9.5126(-06)
	73	7	33	40N	139 E	10078-10605	364.8		255.8			357.4	.061992	184.5	.075487	-1.6219(-06)
	77	5	70	29N	141 E	10054-11195	361.0		252.1			369.8	.058256	235.5	.066050	-1.2019(-06)
	78	5	70	42S	84 W	10000-10201	364.5		255.5			420.1	.037554	1720.4	-.223565	1.2925(-05)
	80	4	0	24N	05 E	10242-11183	368.3		259.4			369.7	.061141	777.0	-.034873	3.5431(-06)
	83	10	33	37N	96 E	10259-10993	365.1		256.1			360.6	.061702	341.1	.045088	-1.4835(-07)
	84	9	17	10S	161 E	10015-11071	367.2		258.1			361.2	.061830	417.0	.031732	4.5460(-07)

TABLE 11

Determined Values of Δ^2 Coefficient

Leg Designation	All	Northwest	South	Average of northwest and south
12.5	-1.7987×10^{-6}	-1.2302×10^{-6}	-2.002×10^{-6}	-1.61×10^{-6}
13.4	-3.2742	-4.1076×10^{-6}	$+2.3056 \times 10^{-6}$	-0.90×10^{-6}
14.5	- .2728	$- .1763 \times 10^{-6}$	$- .6471 \times 10^{-6}$	$+0.23 \times 10^{-6}$
16.3	-2.7563	-3.6711×10^{-6}	-2.1606×10^{-6}	-2.92×10^{-6}
18.2	-3.5162	-2.5448×10^{-6}	-2.0875×10^{-6}	-2.31×10^{-6}
19.5	-1.0117	-7.2053×10^{-6}	-6.8109×10^{-6}	$+0.20 \times 10^{-6}$
22.0	-1.9157	-1.7285×10^{-6}	-2.5919×10^{-6}	-2.16×10^{-6}
24.2	+ .6344	-1.4857×10^{-6}	--	-1.49×10^{-6}
Average of all legs				-1.37×10^{-6}

TABLE 12

Travel-Time Curve

t Statistic on Slope Differences

Equation: $t = a + b$

Leg Designation	Comparison		t	n	P
12.5	NTS→EUS ATL→EUS	(.07930)			
	vs		2.79	36	.01
	NW →US	(.08052)			
	NTS→EUS ATL→EUS	(.07930)	2.88	20	.01
	vs S→US	(.08072)			
	NW→US	(.08052)			
	vs S→US	(.08072)	.32	30	.5
13.4	NW→US	(.07446)			
	vs S→US	(.07504)	1.11	54	.27
14.5	NW→US	(.06952)			
	vs		4.4	80	.005
	S→US	(.06788)			
16.3	NW US	(.06157)			
	vs S→US	(.06125)	.92	80	.35
18.2	NW→US	(.05389)			
	vs S→US		3.6	94	.005
19.5	NW→US	(.05145)			
	vs		.26	56	.8
	S→US	(.05126)			
22.0	NW→US	(.04537)			
	vs S→US	(.04572)			
	NW→WUS	(.04504)			
	vs		1.82	70	.07
	NW→EUS	(.04566)			
	NW WUS	(.04504)			
	vs		3.6	50	.005
	SEML→WUS	(.04710)			
24.2	NW→US	(.04062)			
	ALG→US	(.04077)			
	NW→US	(.4062)	1.22	31	.25
	vs SEML→US	(.4120)			

TABLE 13

Travel-Time Curves (Straight-Line Segments)

Developed by Extrapolation Procedure Described in Text

Leg Designation	All Data	Northwest Data	South Data	Other	δ (sec)
12.5	103.0 + .08030 Δ	102.2 + .08052 Δ	101.5 + .08072 Δ		
13.4	125.0 + .07459 Δ	125.4 + .07446 Δ	122.6 + .07504 Δ (125.1)		
14.5	153.0 + .06880 Δ	149.2 + .06952 Δ	156.9 + .06788 Δ (147.9) 159.6 + .06788 Δ (150.6)		
16.3	197.8 + .061400 Δ	197.5 + .06157 Δ	200.0 + .06125 Δ (197.9)	196.9 + .06157 Δ (Novaya Zemlya) 197.2 + .06157 Δ (Algeria)	(-.4)
18.2	244.9 + .05488 Δ	253.0 + .05392 Δ	240.0 + .05558 Δ (253.0)	253.2 + .053923 Δ (Novaya Zemlya) 249.4 + .05392 Δ (LONG SHOT) 253.5 + .05392 Δ (Algeria)	(+.4)
19.5	273.8 + .05133 Δ	273.3 + .05145 Δ	274.6 + .05126 Δ (273.0)		
22.0	326.5 + .04541 Δ	327.4 + .04537 Δ	324.2 + .045720 Δ (327.4)	328.1 + .04537 Δ (Semipalatinsk) 328.4 + .04537 Δ (Algeria)	(+.9)
24.2	367.1 + .04127 Δ	374.2 + .04062 Δ		375.6 + .04062 Δ (Semipalatinsk) 375.6 + .04062 Δ (Algeria)	(+1.4)

TABLE 14

Travel-Time Curve - EC-SL I

Distance Range (km)	Equation of Travel-Time Curve (in km)
0-230.4	T = .166667
230.4-2206.8	T = 11.1 + .118500 Δ 8.5
2206.8-2678.4	T = 60.1 + .096296 Δ 10.4
2678.4-3835.8	T = 103.6 + .080055 Δ 12.5
3835.8-4937.4	T = 124.6 + .074502 Δ 13.4
4937.4-5958.3	T = 152.5 + .068912 Δ 14.5
5958.3-7313.0	T = 196.8 + .061477 Δ
7313.0-8303.9	T = 244.4 + .054968 Δ
8302.9-8867.8	T = 270.8 + .051750 Δ
8867.8-10006.8	T = 327.9 + .045311 Δ
10006.8-11200	T = 372.2 + .040884 Δ

Distances are given so that times agree at crossings to .01 seconds.

If you need to round travel-time curve at crossings for use in program, do as little smoothing as possible.

TABLE 15

Travel-Time Curve - EC-SL II

Distance Range (km)	Equation of Travel-Time Curve (in km)
0-230-4	T = .166667
230.4-2166.3	T = 11.1 + .118500
2166.3-2678.4	T = 59.2 + .096296
2678.4-3853.8	T = 102.7 + .080055
3853.8-4973.2	T = 124.1 + .074502
4973.2-6039.0	T = 151.9 + .068912
6039.0-7328.3	T = 196.8 + .061477
7328.3-8172.8	T = 244.5 + .054968
8172.8-8867.8	T = 270.8 + .051750
8867.8-10006.8	T = 327.9 + .045311
10006.8-11200	T = 372.2 + .040884

Distances are given so that times agree at crossings to .01 seconds. If you need to round travel-time curve at crossings for use in program, do as little smoothing as possible.

TABLE 16

TRAVEL-TIME CURVE EC-CU I

Apply indicated changes to travel-time curve EC-SL I. Make smooth travel-time curve between points given.

km	Travel-Time Changes	km	Travel-Time Changes
2650	00 sec	7100	-.20 sec
2700	-.42	7250	-.37
2750	-.23	7450	-.08
2835	00	7700	-.04
3100	+.10	7850	00
3425	+.07	8100	00
3620	00	8210	-.15
3725	-.24	8300	-.03
3900	-.27	8335	-.02
4000	00	8600	-.01
4100	+.06	8750	-.10
4325	+.10	8825	-.22
4500	+.07	8900	-.16
4675	00	9000	-.04
4800	-.09	9100	-.02
4900	-.25	9200	+.02
5030	-.07	9300	+.02
5100	00	9600	00
5225	+.05	9750	-.01
5425	+.04	9850	-.04
5550	00	9985	-.13
5775	-.25	10060	-.15
5950	-.42	10150	-.09
6075	00	10250	-.04
6300	+.05	10375	00
6475	+.08	10500	+.03
6650	+.12	10700	+.02
6760	+.08	10900	+.01
6910	00	11200	00

Example of calculation of travel-time for EC-CU I travel-time curve:

$$4900^{T}_{\text{EC-CU I}} = 4900^{T}_{\text{EC-SL I}} - 0.25 = 124.90 + 365.06 - 0.25 = 489.71$$

TABLE 17

TRAVEL-TIME CURVE EC-CU II

Apply indicated changes to travel-time curve EC-SL II. Make smooth travel-time curve betweer points given.

km	Travel-Time Changes	km	Travel-Time Changes
2650	00 sec	7100	-.18 sec
2700	-.42	7250	-.35
2750	-.23	7450	-.10
2835	00	7700	-.04
3100	+.10	7850	00
3425	+.07	8100	00
3590	00	8210	-.12
3725	-.19	8300	-.03
3900	-.25	8335	-.02
4000	00	8600	-.01
4100	+.06	8750	-.10
4325	+.10	8825	-.22
4500	+.07	8900	-.16
4675	00	9000	-.04
4800	-.09	9100	-.02
4900	-.18	9200	+.02
5030	-.07	9300	+.02
5100	00	9600	00
5225	+.05	9750	-.01
5425	+.04	9850	-.04
5550	00	9985	-.13
5775	-.20	10060	-.15
5950	-.35	10150	-.09
6200	00	10250	-.04
6300	+.05	10375	00
6475	+.08	10500	+.03
6650	+.12	10700	+.02
6760	+.08	10900	+.01
6850	00	11200	00

Example of calculation of travel-time for EC-CU II Travel-time curve:

$$4900^{T}\text{EC-CU II} = 4900^{T}\text{EC-SL II} - 0.18 = 124.10 + 365.06 - 0.18 = 488.98$$

TABLE 18

Epicenter Locations by Various Travel Time Curves
Worldwide Data

Herrin-67		EC-CU-I		EC-CU-II	
Latitude	Longitude	Latitude	Longitude	Latitude	Longitude
45°04.5'N	149°27.9'E	45°10.9'N	149°28.1'E	45°01.4'N	149°28.7'E
44°45.8'N	149°59.4'E	44°48.3'N	149°57.7'E	44°47.3'N	149°58.1'E
51°11.1'N	179°19.6'N	51°07.6'N	179°13.3'W	51°08.7'N	179°15.4'W
54°13.7'N	168°11.7'E	54°12.5'N	168°15.7'E	54°13.8'N	168°14.0'E
30°32.4'N	137°35.4'E	30°32.5'N	137°38.2'E	30°30.5'N	137°35.2'E
27°29.4'S	063°30.3'W	27°29.3'S	063°14.8'W	27°29.4'S	063°15.1'W
17°45.4'N	094°11.9'W	17°44.3'N	094°09.4'W	17°44.8'N	094°10.2'W
27°16.4'N	127°23.2'E	27°15.0'N	127°15.6'E	27°15.1'N	127°24.8'E
13°45.5'S	069°18.2'W	13°47.9'S	069°13.4'W	13°47.5'S	069°14.8'W
18°36.7'N	069°19.4'W	18°34.8'N	069°28.0'W	18°35.7'N	069°24.9'W
07°21.0'N	035°48.9'W	07°20.3'N	035°49.9'W	07°20.6'N	035°48.7'W
59°27.3'N	152°03.2'W	59°24.4'N	151°57.0'W	59°26.3'N	151°59.9'W
56°23.2'N	153°59.6'W	56°22.3'N	153°54.6'W	56°23.1'N	153°56.2'W
60°23.8'N	140°52.4'W	60°19.8'N	140°50.3'W	60°22.9'N	140°53.8'W
50°47.8'N	130°06.9'W	50°44.9'N	130°00.1'W	50°46.2'N	130°03.6'W
56°40.3'N	152°56.8'W	16°16.4'S	071°26.4'W	16°16.0'S	071°25.9'W
44°31.6'N	031°15.3'N	44°32.2'N	031°15.3'W	44°32.2'N	031°15.9'W
51°44.4'N	178°11.2'E	51°41.9'N	178°08.5'E	51°42.7'N	178°09.0'E
50°11.5'N	176°57.9'W	50°10.0'S	176°52.0'W	50°10.4'N	176°54.1'W
10°37.0'S	078°02.6'W	10°33.3'S	077°54.9'W	10°35.7'S	077°56.4'W
53°15.4'N	159°40.3'E	53°15.6'N	159°42.0'E	53°15.8'N	159°42.2'E
05°36.3'S	076°55.1'W	05°31.8'S	076°51.5'W	05°33.1'S	076°53.3'W
53°55.3'N	160°26.5'E	53°56.4'N	160°27.1'E	53°54.6'N	160°27.0'E
06°41.5'N	073°00.1'W	06°40.1'N	073°06.5'W	06°39.3'N	073°06.0'W
04°08.4'N	076°17.1'W	04°10.3'N	076°24.1'W	04°08.7'N	076°23.0'W
19°20.7'N	155°26.3'W	19°23.0'N	155°19.6'W	19°26.3'N	155°26.7'W
51°19.6'N	179°21.6'W	51°17.4'N	179°16.5'W	51°19.6'N	179°17.8'W
41°15.1'N	144°32.7'E	41°14.4'N	144°17.8'E	41°15.2'N	144°18.4'E
40°32.9'N	139°03.7'E	40°29.0'N	139°00.5'E	40°31.8'N	139°04.2'E
15°58.0'S	173°15.4'W	15°57.2'S	173°16.5'W	15°58.4'S	173°14.6'W
32°08.7'N	131°44.7'E	32°06.0'N	131°42.2'E	32°07.4'N	131°42.7'E
29°01.0'N	140°54.0'E	28°59.8'N	140°50.0'E	29°02.0'N	140°53.4'E
41°47.2'S	083°44.0'W	41°51.8'S	083°38.0'W	41°51.4'S	083°32.7'W
13°32.7'N	089°56.3'W	13°31.3'N	089°58.6'W	13°27.9'N	089°56.0'W

TABLE 19

Epicenter Shifts When Using LRSM Data and Different Travel-Time Curves

(Depth Restrained to Nearly Correct Value)

Event Location (World-Wide Data)		Range (Degrees) (LRSM/U.S.)	Number of LRSM Stations	Semi-Major Axis (km)	EC-CU-I (km)				EC-CU-II (km)			
					Far	Near	Right	Left	Far	Near	Right	Left
45°01'N	149°29'E	66-87	25	55	35			19	36			19
50°20'N	177°03'W	40-66	19	58		40		4	10		2	
44°47'N	149°58'E	68-87	20	57	57			18	47			22
54°14'N	168°14'E	49-71	16	46		28	6		94			6
54°42'N	159°39'W	31-56	24	45	[illegible]		4		61		4	
51°42.N	170°54'W	44-50	6	197		156	12			108	16	
42°31'N	137°35'E	83-90	11	230	136		18		140			8
27°29'S	063°15'W	67-83	13	76		10	20			12	24	
52°13'N	175°30'E	44-68	13	78		46		20		24		20
52°06'N	169°33'W	38-61	13	57		16	26		60		26	
30°38'N	131°01'E	85-99	16	133	184			32	184			32
27°15'N	127°25'E	90-96	6	520	184			56	32		100	
13°48'S	069°15'W	57-64	7	259		130			56		110	
18°36'N	069°25'W	22-45	21	26	23			2		6		20
07°21'N	035°49'W	48-82	17	51	26			36	44			36
56°23'N	153°56'W	30-52	18	47		20	12		29		17	
59°44'N	148°50'W	29-48	18	45	44			2	58			2
56°38'N	152°53'W	30-51	16	50	18			4	36			3
16°16'S	071°26'W	54-71	20	57		52		6		[illegible]	6	
50°10'N	176°54'W	40-66	20	59		9		11	40			5
53°16'N	159°42'E	48-74	8	110	180			30	180			30
50°33'S	076°53'W	47-58	14	111		100	12		20		10	
60°39'N	073°06'W	36-54	18	77		30		8		24	8	
40°09'N	076°23'W	34-53	19	66		50				30	6	
19°26'N	155°27'W	36-58	17	58	3		10		70		8	
51°20'N	179°18'W	44-67	12	66		50	18		20		15	
41°15'N	144°18'E	68-92	23	52	17		15			4	20	
40°32'N	139°04'E	75-94	18	57	18		34		18		34	
40°22'N	138°53'E	75-95	18	54	2		34		4		34	
32°07'N	131°43'E	84-98	16	109	68		100		70		104	
29°02'N	140°53'E	81-101	17	116	46		10		52		10	

TABLE 20

Epicenter Shifts

Events for Which Semi-Major Axis is Less Than 60 Kilometers

Range of LRSM Stations (degrees)	EC-CU-1		EC-CU-II	
	FAR (km)	NEAR (km)	FAR (km)	NEAR (km)
40-66		40 (in)	10 (in)	
49-71		28 (in)	94 (out)	
31-56	61 (out)		61 (out)	
38-61		16 (out)(in/.5)	60 (out)	
22-45	23 (in)			6 (out)
48-82	26 (in)		44 (out)	
30-52		20 (in)	29 (out)	
29-48	44 (out)		58 (out)	
30-51	18 (in)		36 (in)	
54-71		52 (out)(in/.5)		16 (in)
40-66		9 (in)	40 (in)	
36-58	3 (in)		70 (out)	
	175	165	502	22

OUT - Location outside 95% CHI^2 Ellipse (S.D. = 0.4 sec)

IN - Location inside 95% CHI^2 Ellipse (S.D. = 0.4 sec)

EC-CU-I: (175-165) /12 = 1 km FAR

EC-CU-II: (502-22) /12 = 40 km FAR

TABLE 21

Noise and Relative Signal Levels

Station	Geology	Noise Level (mμ)	Magnitude (MISSISSIPPI = 4.75)	Relative Signal Amplitude (mμ)	Relative Signal Amplitude/Noise
AZ-TX	Dolomite (Paleozoic)	23	-.23	.59	.026
BL-WV	Sandstone (Paleozoic)	28	+.06	1.15	.041
BR-PA	Sandstone (Paleozoic)	10	0	1.00	.100
BX-UT	Sandstone (Mesozoic)	2.7	-.24	.58	.213
CP-CL	Granite	6.5	-.45	.35	.054
CU-NV	Limestone (Paleozoic)	10	-.30	.50	.050
DH-WY	Sandstone (Paleozoic)	21	+.11	1.29	.061
DR-CO	Granite	1.5	-.54	.29	.193
DU-OK	Granite (700')	8.5	-.19	.65	.076
EB-MT	Granite	50	+.06	1.15	.023
EK-NV	Limestone (Paleozoic)	2.5	-.30	.50	.200
FR-MA	Sediment (Tertiary)	55	+.15	1.41	.026
GI-MA	Sediment (Tertiary)	23	+.24	1.74	.076
GV-TX	Sediment (Tertiary)	70	-.09	.81	.012
HH-ND	Shale (Mesozoic)	30	+.32	2.09	.070
HL-ID	Metamorphic (Granitic)	1.5	-.35	.45	.300
HM-ME	Metamorphic (Mesozoic)	2.8	-.10	.79	.282
LC-NM	Limestone (Paleozoic)	5	-.23	.59	.118
LS-NH	Metamorphic	20	-.06	.87	.044
MH-NV	Metamorphic & Granite	5	-.23	.59	.118
MV-CL	Metamorphic	8	-.25	.56	.070
RK-ON	Granite	50	+.22	1.66	.033
RT-MM	Limestone (Mesozoic)	8	-.17	.68	.085
RY-ND	Sediment (Tertiary)	25	+.38	2.40	.096
SK-TX	Sediment (Paleozoic)	10	-.01	.98	.098
WI-NV	Limestone & Metamorphic (Mesozoic)	2.5	-.33	.47	.188
[illegible]	Granite	2.0	-.36	.45	.230
[illegible]	Granite	3.0	-.28	.53	.177
UBSO	Sandstone (Tertiary)	4.	-.07	.85	.213
TPSO	Granite	1.8	-.36	.45	.250
CPSO	Limestone (Paleozoic)	10.0	-.04	.91	.091

TABLE 22

Slope of Amplitude vs Distance Curve

Equation: $\log A/T = \alpha + \beta \log \Delta$

Leg Designation	β-Values (Standard Deviation of Residuals)			
	All Data (Uncorrected)	All Data (corrected)	Northwest	South
12.5	- 1.9 (.22)	- 2.5 (.18)	--	--
13.4	+ 2.6 (.27)	+ 1.7 (.21)	+ 1.9 (.21)	+ 1.0 (.24)
14.5	+ 0.2 (.34)	+ .3 (.23)	+ 0.5 (.26)	- 1.6 (.25)
16.3	+ 0.1 (.26)	+ .8 (.20)	+ 2.0 (.22)	+ 0.7 (.21)
18.2	- 7.2 (.29)	- .6 (.20)	- 1.8 (.20)	- 3.1 (.20)
19.5	- .8 (.19)	- 1.5 (.17)	- 4.2 (.17)	- 0.1 (.18)
22.0	+ 4.2 (.23)	- 4.6 (.17)	- 3.3 (.17)	- 0.1 (.15)
24.2	-11.3 (.29)	-12.3 (.25)	- 8.5 (.29)	

TABLE 23

log A/T vs Δ

At 2700 km, log A/T = 3.00

Leg	Equation
12	log A/T = 11.50 - 2.48 log Δ
13	= -3.10 + 1.65 log Δ
14	= 1.60 + .30 log Δ
16	= - .25 + .77 log Δ
18	= 5.40 + .65 log Δ
19	= 8.95 - 1.55 log Δ
22	= 21.15 - 4.57 log Δ
25	= 51.80 -12.3 log Δ

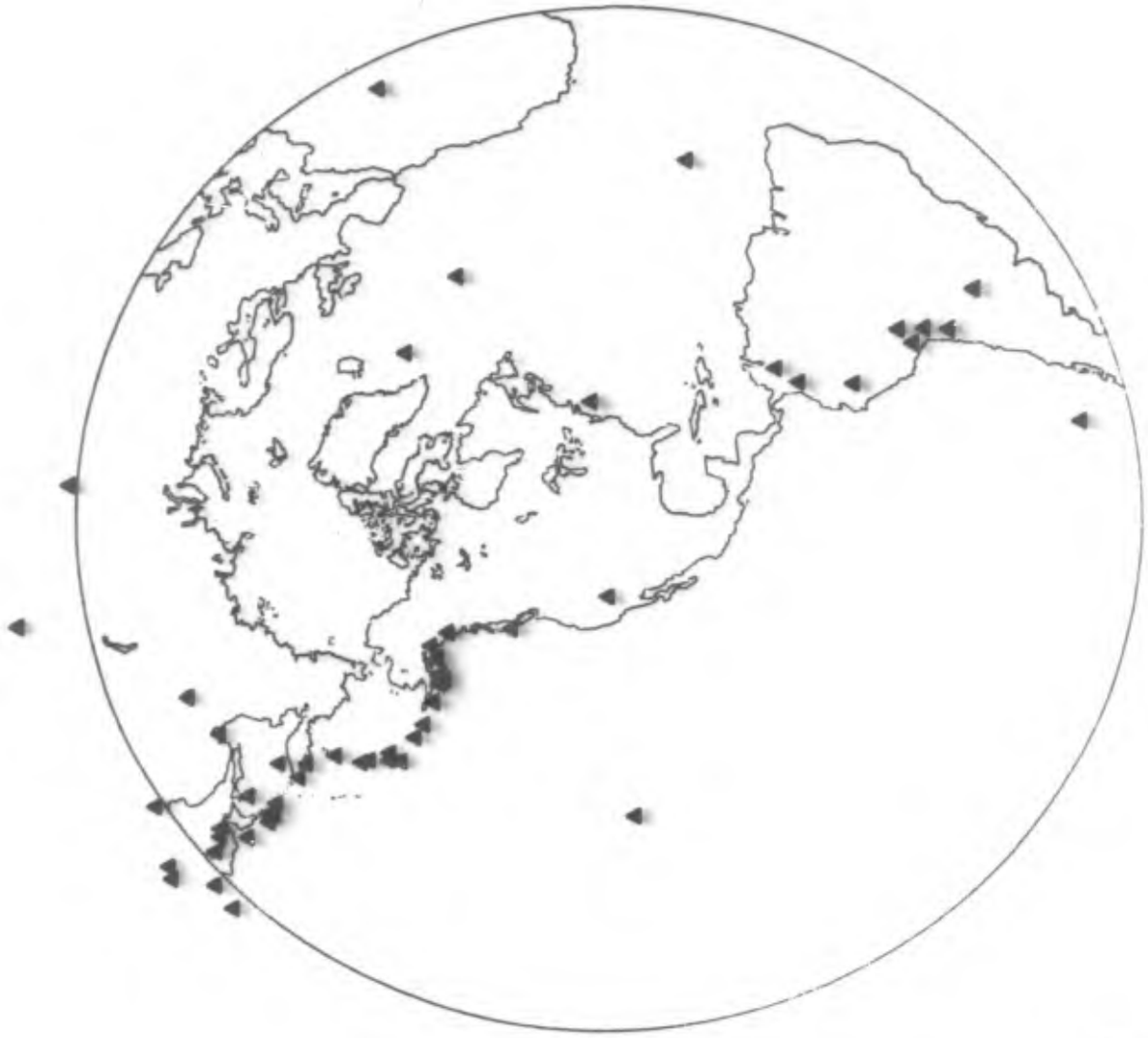

Figure 1

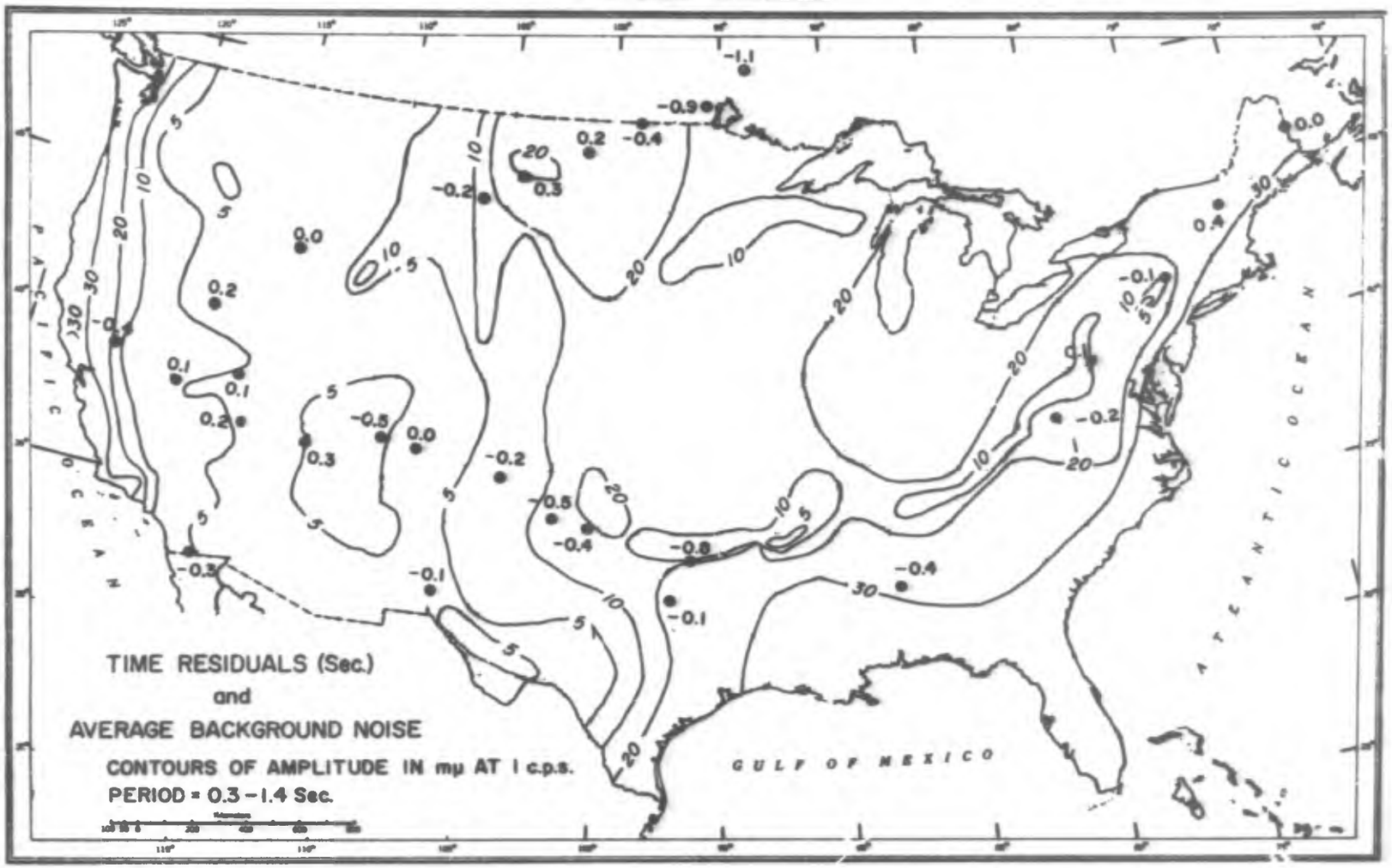
UNITED STATES
TIME RESIDUALS (Sec.)
and
AVERAGE BACKGROUND NOISE
CONTOURS OF AMPLITUDE IN mμ AT 1 c.p.s.
PERIOD = 0.3 – 1.4 Sec.
GULF OF MEXICO
ATLANTIC OCEAN

Figure 2

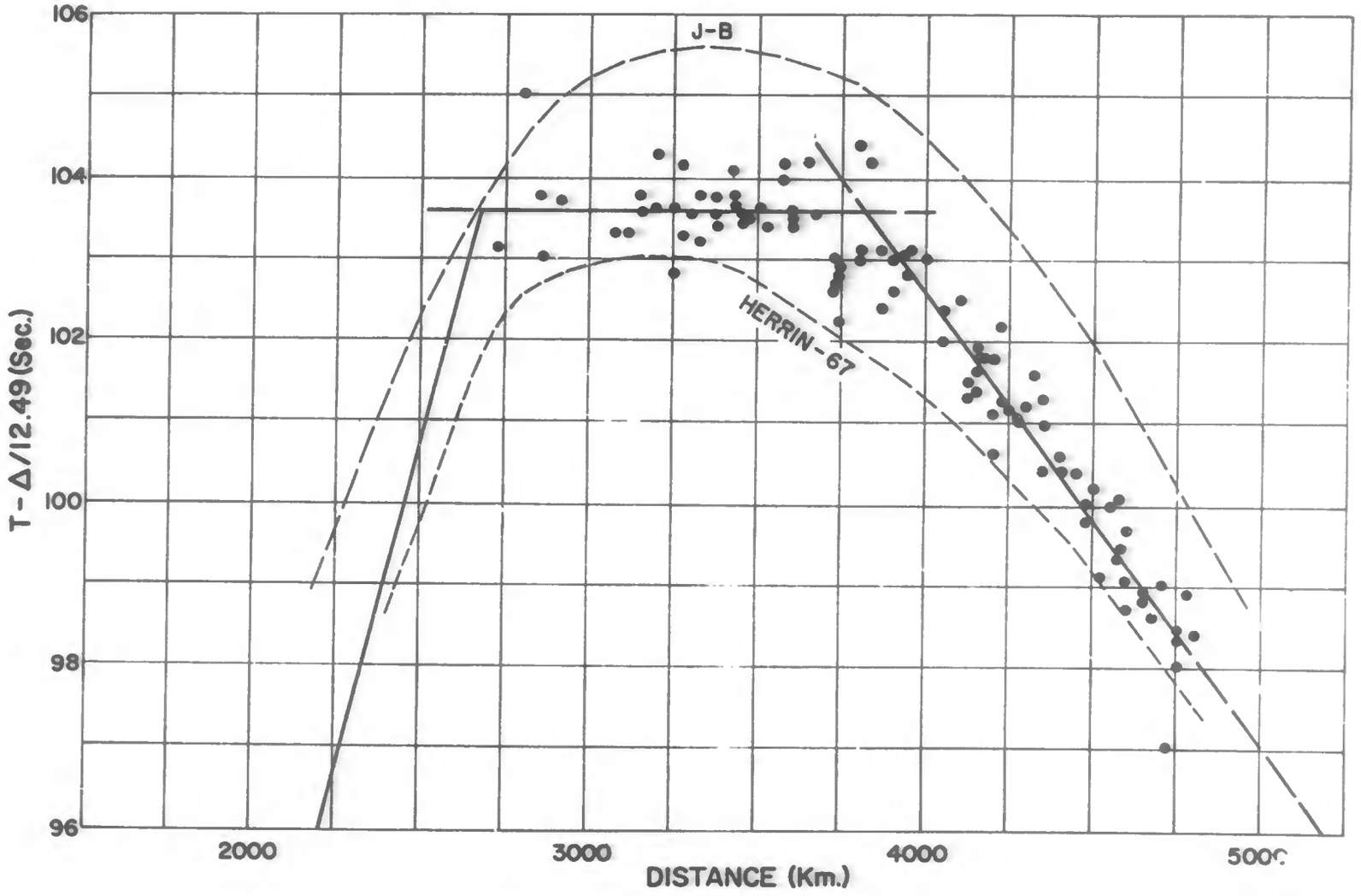
J-B
HERRIN-67
106
104
102
100
98
96
T - Δ/12.49 (Sec.)
2000
3000
4000
5000
DISTANCE (Km.)

Figure 3

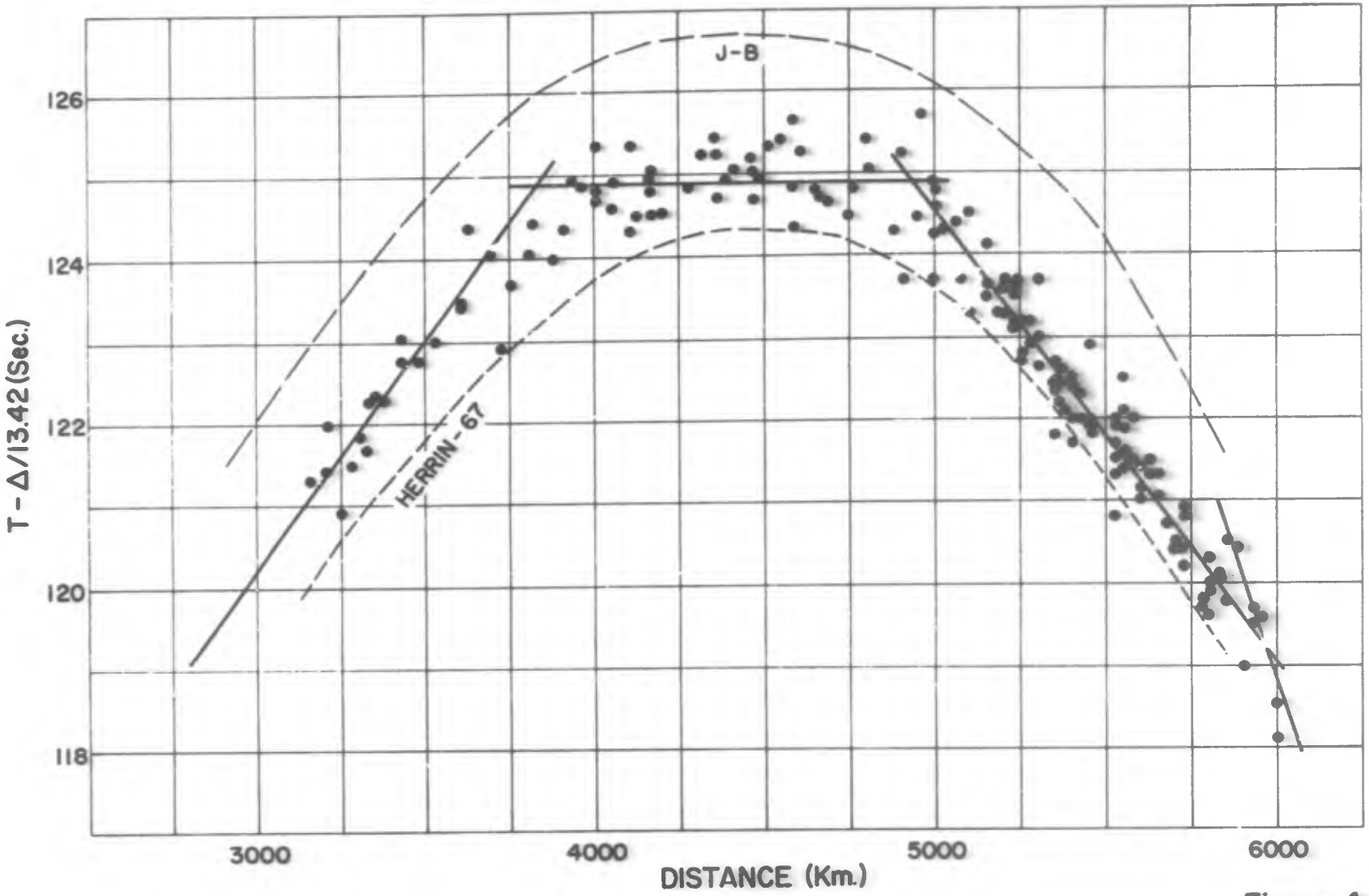
J-B
HERRIN-67
126
124
122
120
118
T-Δ/13.42(Sec.)
3000
4000
5000
6000
DISTANCE (Km.)

Figure 4

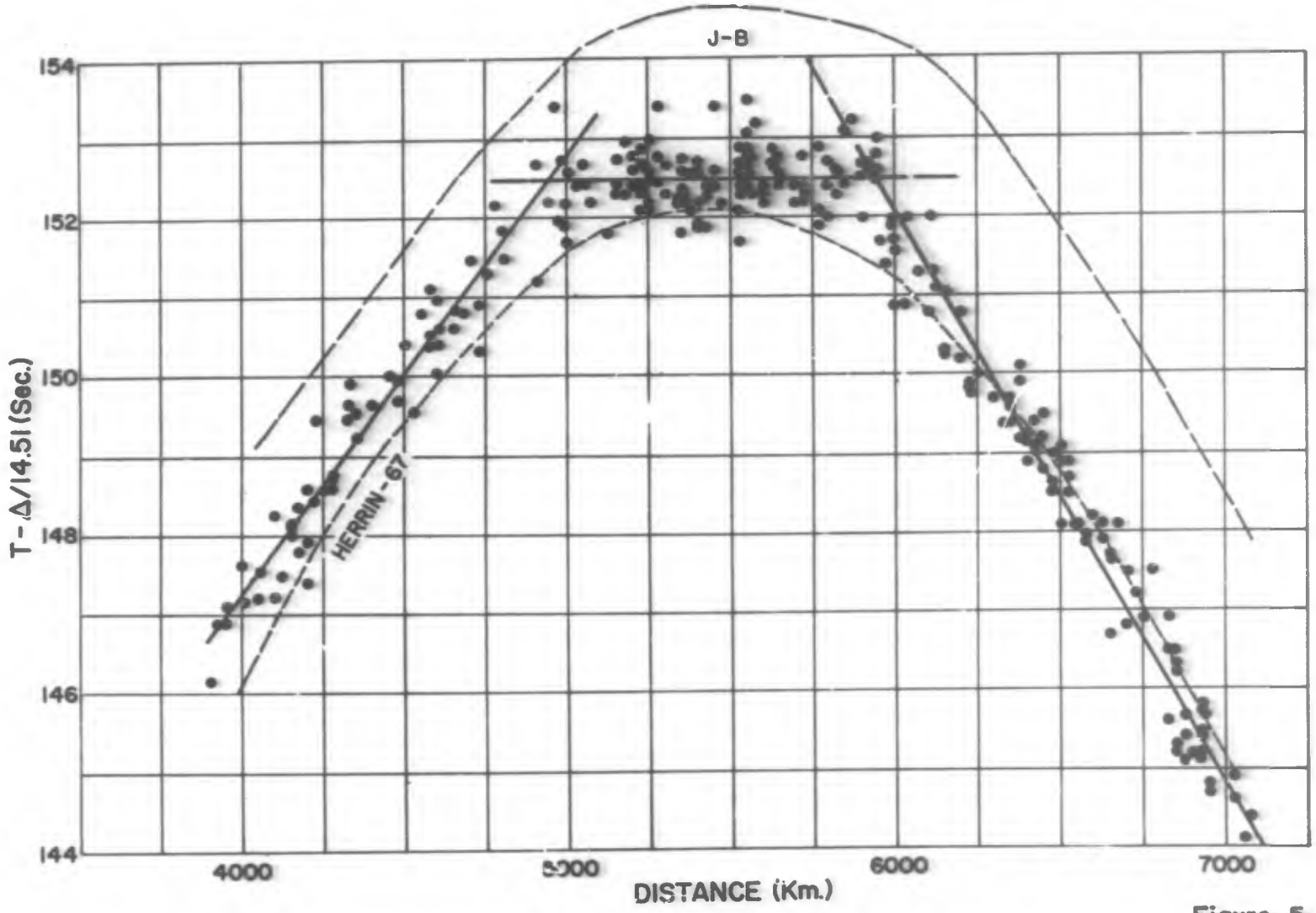
J-B
HERRIN-67
154
152
150
148
146
144
T-Δ/14.51 (Sec.)
4000
5000
6000
7000
DISTANCE (Km.)

Figure 5

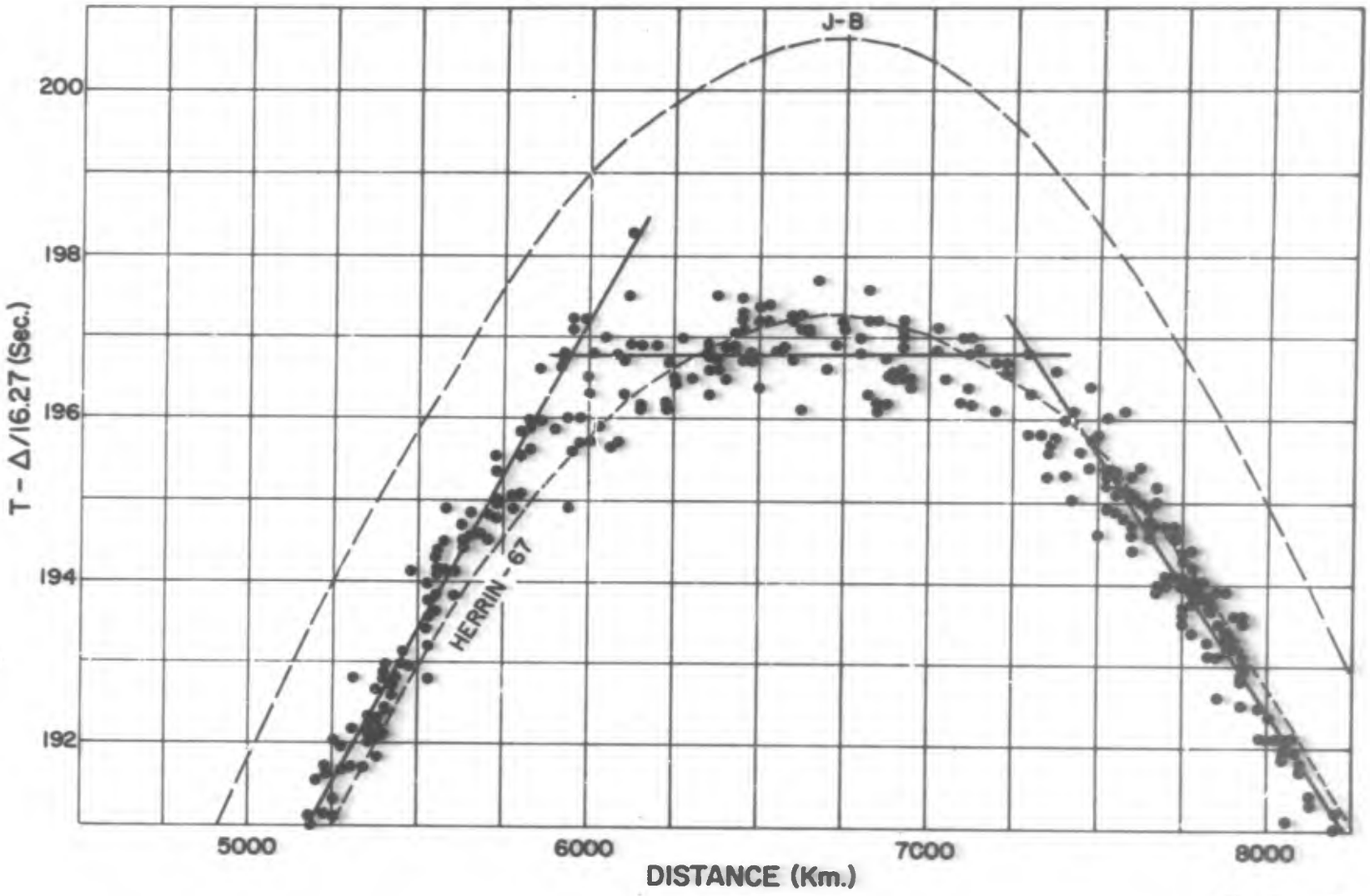
J-B
HERRIN - 67
200
198
196
194
192
T - Δ/16.27 (Sec.)
5000
6000
7000
8000
DISTANCE (Km.)

Figure 6

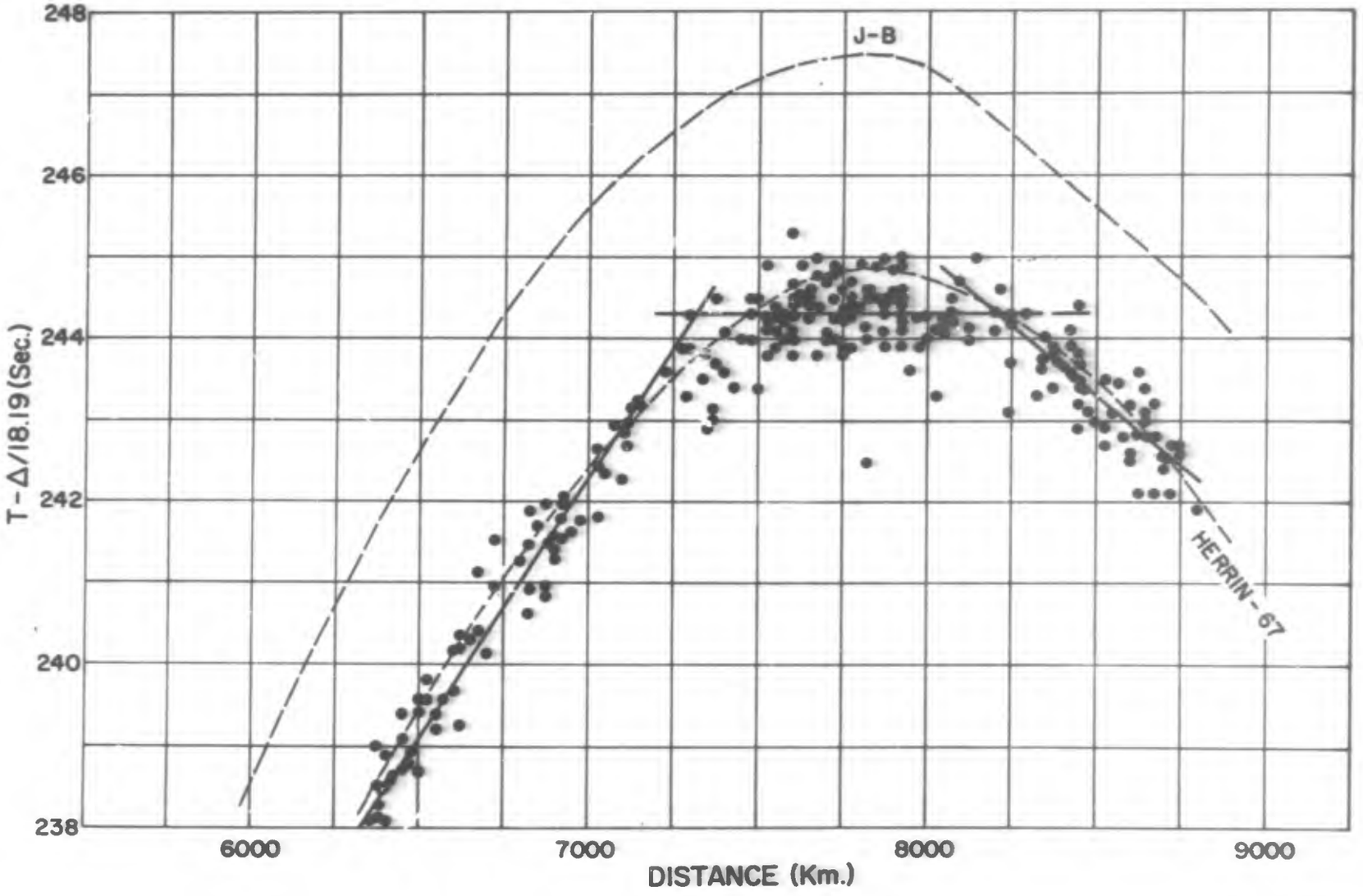
248
246
244
242
240
238
T-Δ/18.19 (Sec.)
6000
7000
8000
9000
DISTANCE (Km.)
J-B
HERRIN-67

Figure 7

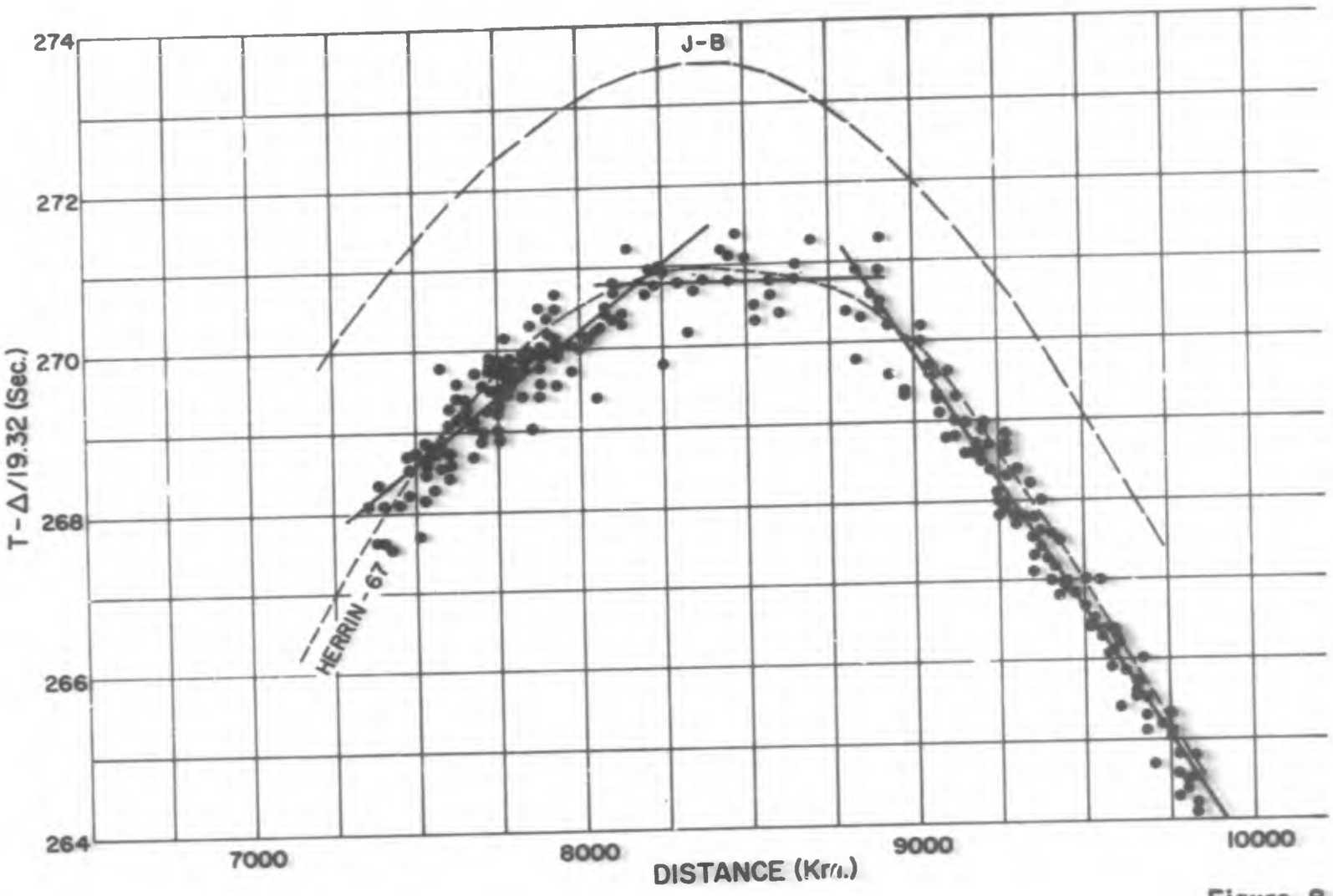
274
272
270
268
266
264
T - Δ/19.32 (Sec.)
J-B
HERRIN - 67
7000
8000
9000
10000
DISTANCE (Km.)

Figure 8

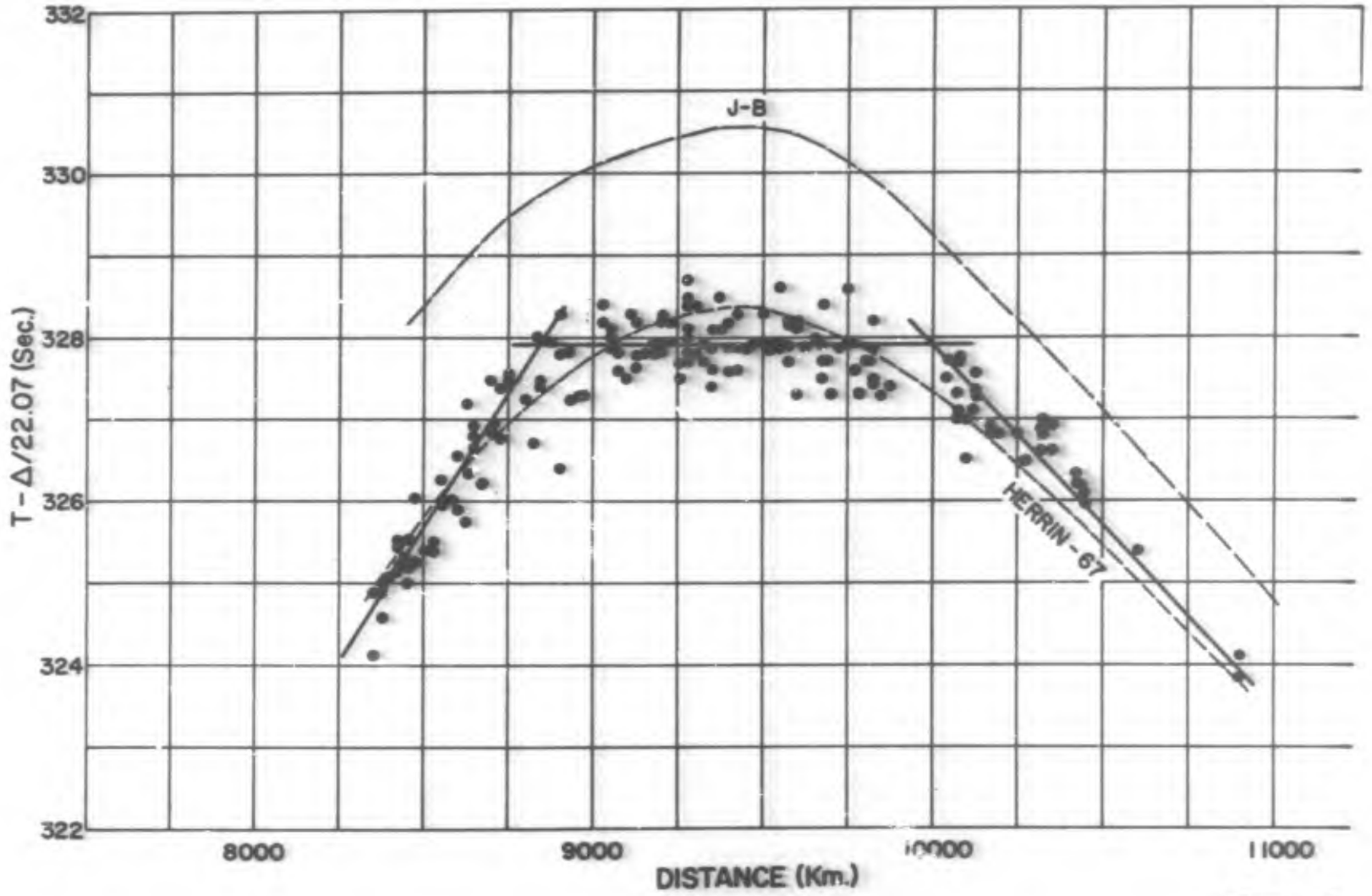
332
330
328
326
324
322
T - Δ/22.07 (Sec.)
J-B
HERRIN - 67
8000
9000
10000
11000
DISTANCE (Km.)

Figure 9

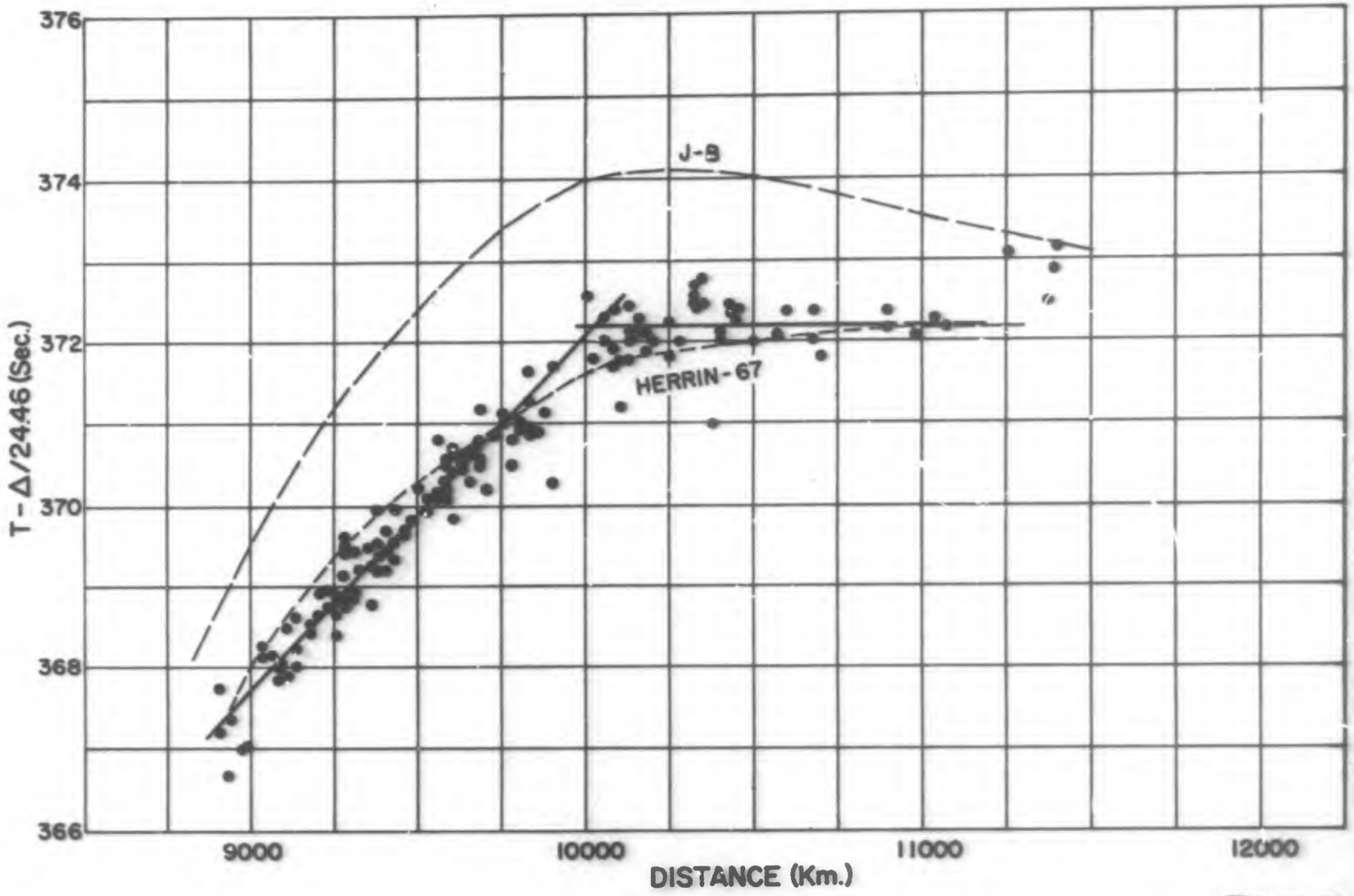
376
374
372
370
368
366
T - Δ/24.46 (Sec.)
J-B
HERRIN-67
9000
10000
11000
12000
DISTANCE (Km.)

Figure 10

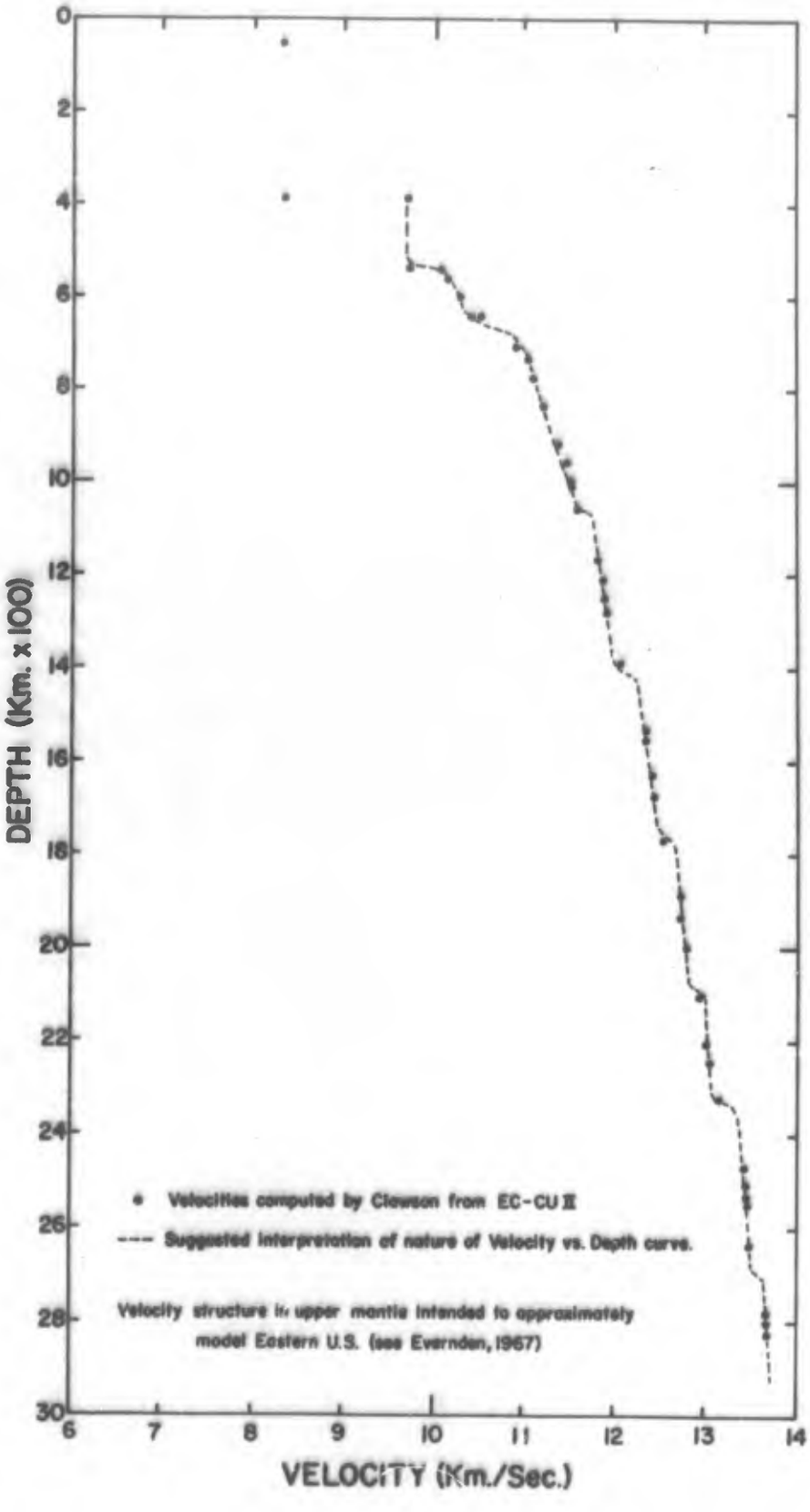
DEPTH (Km. x 100)
0
2
4
6
8
10
12
14
16
18
20
22
24
26
28
30
6
7
8
9
10
11
12
13
14
VELOCITY (Km./Sec.)
Velocities computed by Clawson from EC-CU II
Suggested interpretation of nature of Velocity vs. Depth curve.
Velocity structure in upper mantle intended to approximately model Eastern U.S. (see Evernden, 1967)

Figure 11

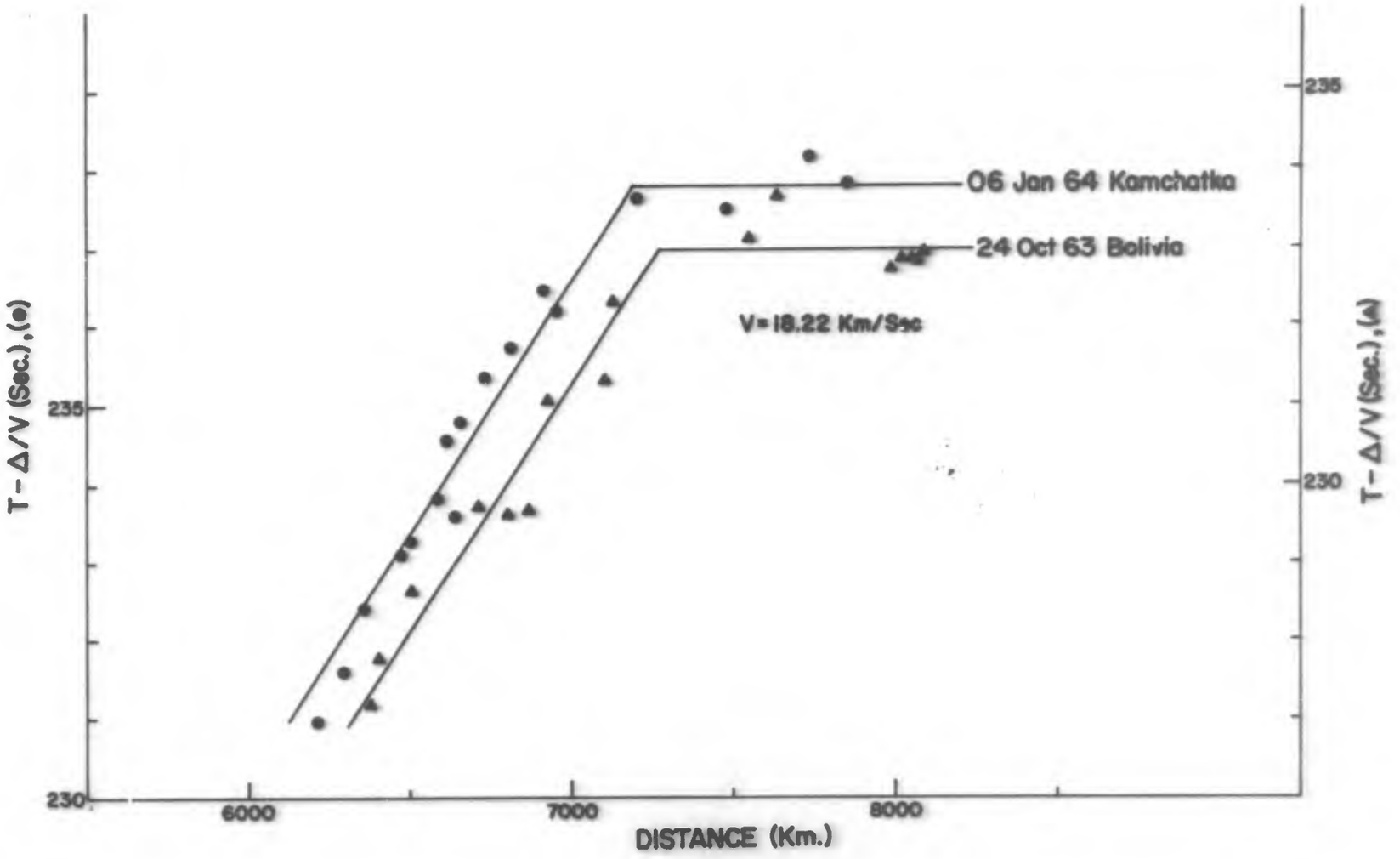
06 Jan 64 Kamchatka
24 Oct 63 Bolivia
V=18.22 Km/Sec
T-Δ/V (Sec.),(●)
T-Δ/V (Sec.),(▲)
235
230
6000
7000
8000
DISTANCE (Km.)

Figure 12

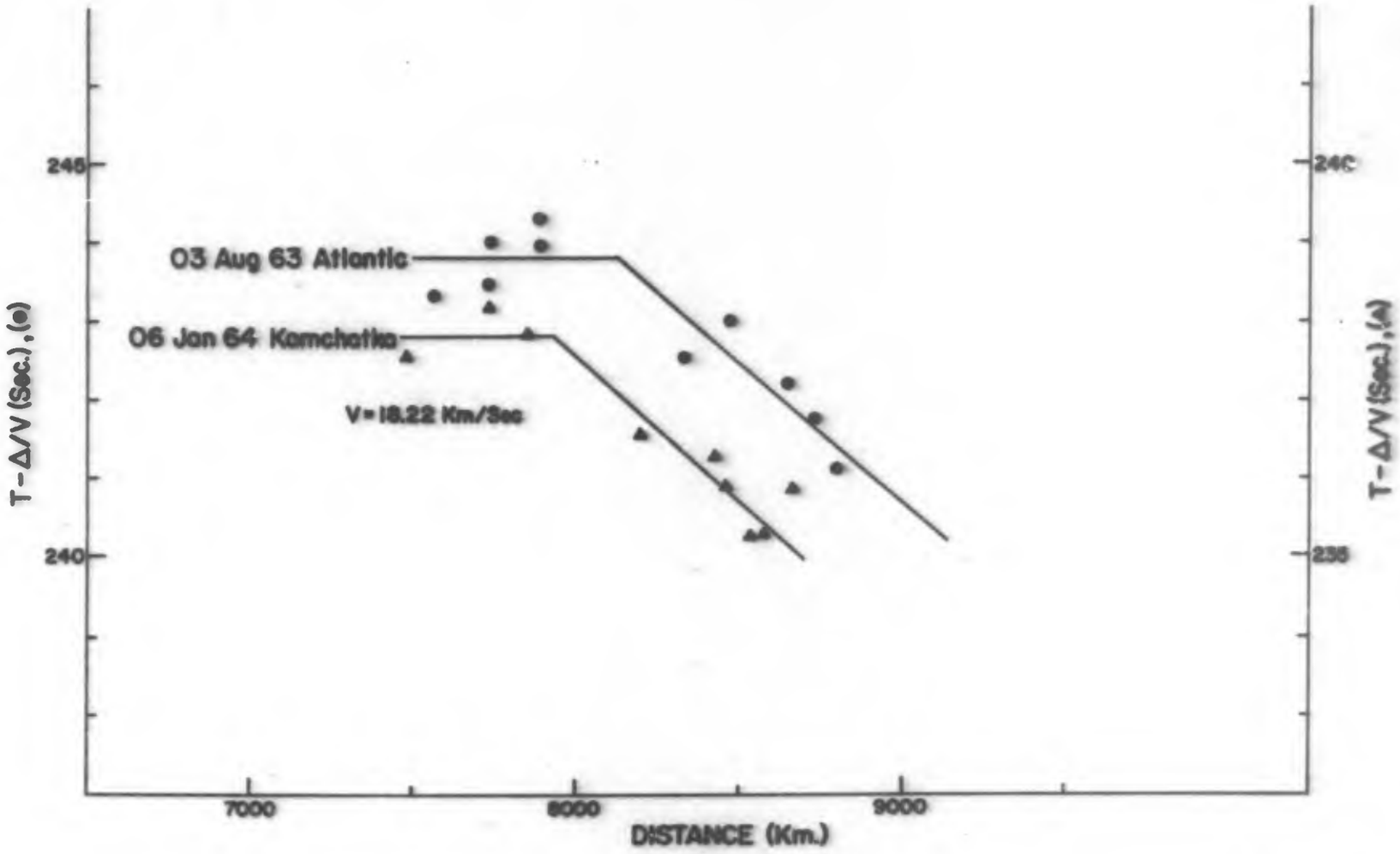
245
240
240
235
03 Aug 63 Atlantic
06 Jan 64 Kamchatka
V = 18.22 Km/Sec
T-Δ/V (Sec.),(o)
T-Δ/V (Sec.),(A)
7000
8000
9000
DISTANCE (Km.)

Figure 13

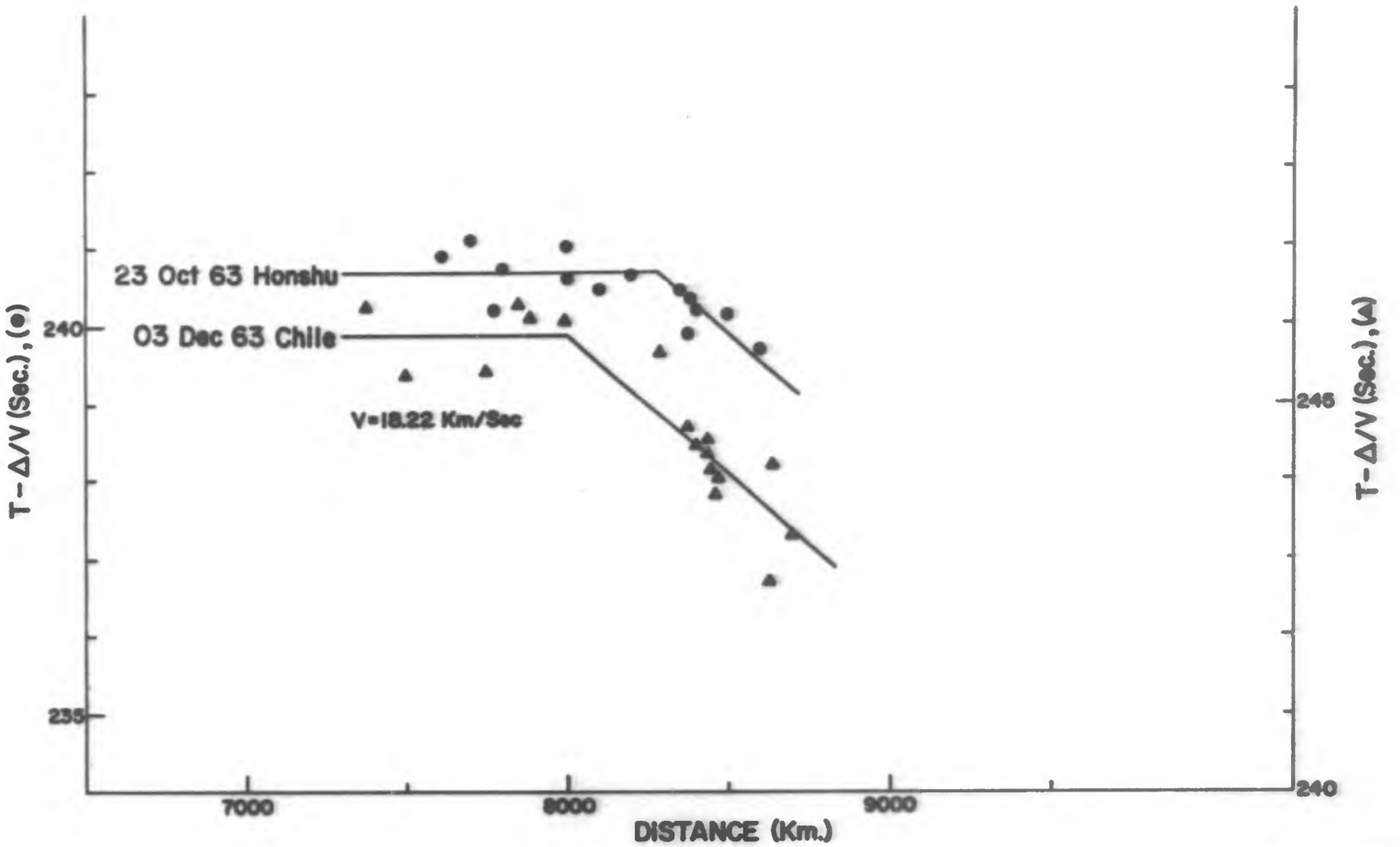
23 Oct 63 Honshu
03 Dec 63 Chile
V=18.22 Km/Sec
T-Δ/V (Sec.), (●)
T-Δ/V (Sec.), (▲)
240
235
245
240
7000
8000
9000
DISTANCE (Km.)

Figure 14

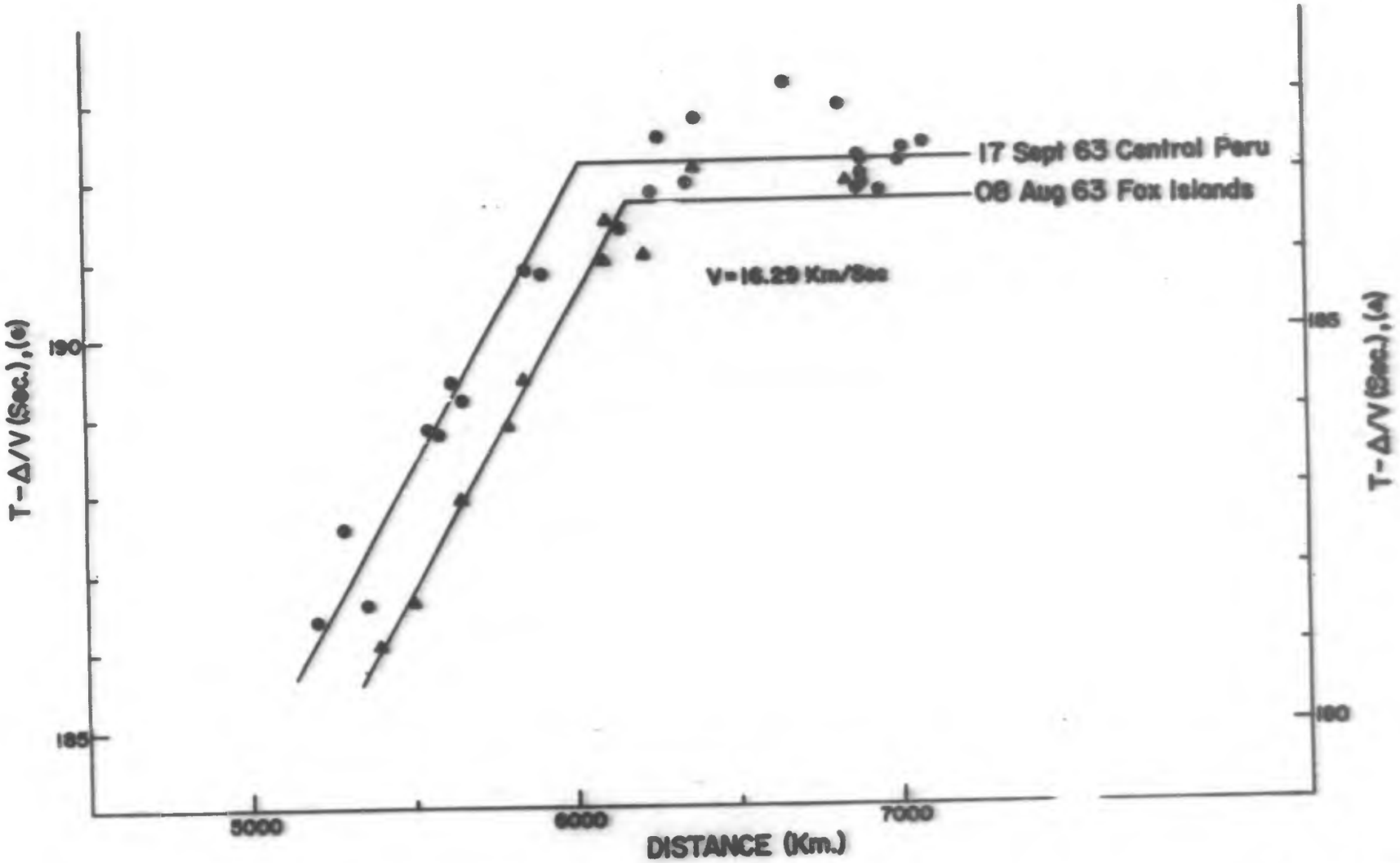
17 Sept 63 Central Peru
08 Aug 63 Fox Islands
V=16.29 Km/Sec
T-Δ/V (Sec.),(s)
T-Δ/V (Sec.),(s)
190
185
185
180
5000
6000
7000
DISTANCE (Km.)

Figure 15

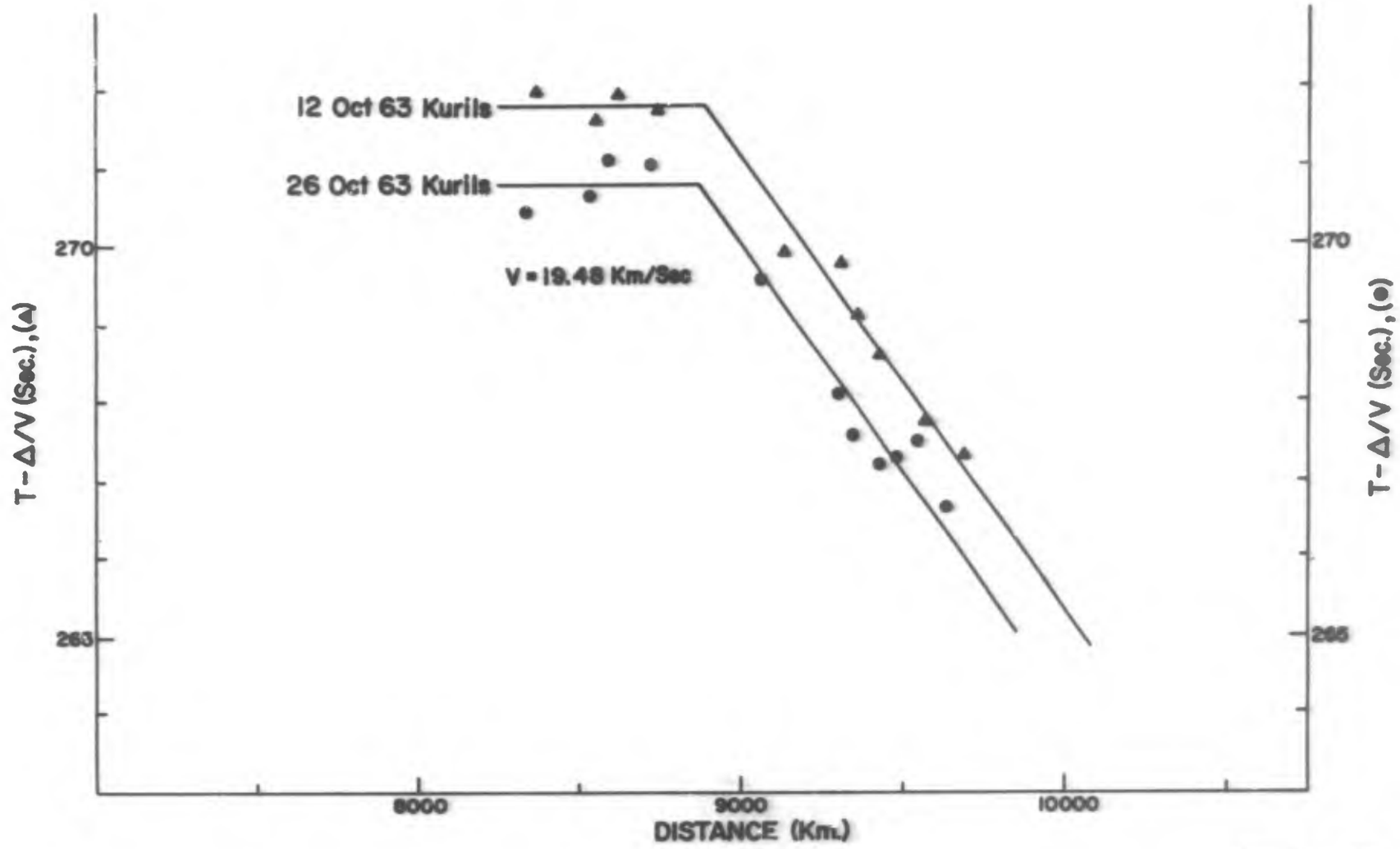
12 Oct 63 Kurils
26 Oct 63 Kurils
V = 19.48 Km/Sec
270
263
T-Δ/V (Sec.),(Δ)
T-Δ/V (Sec.),(●)
8000
9000
10000
DISTANCE (Km.)

Figure 16

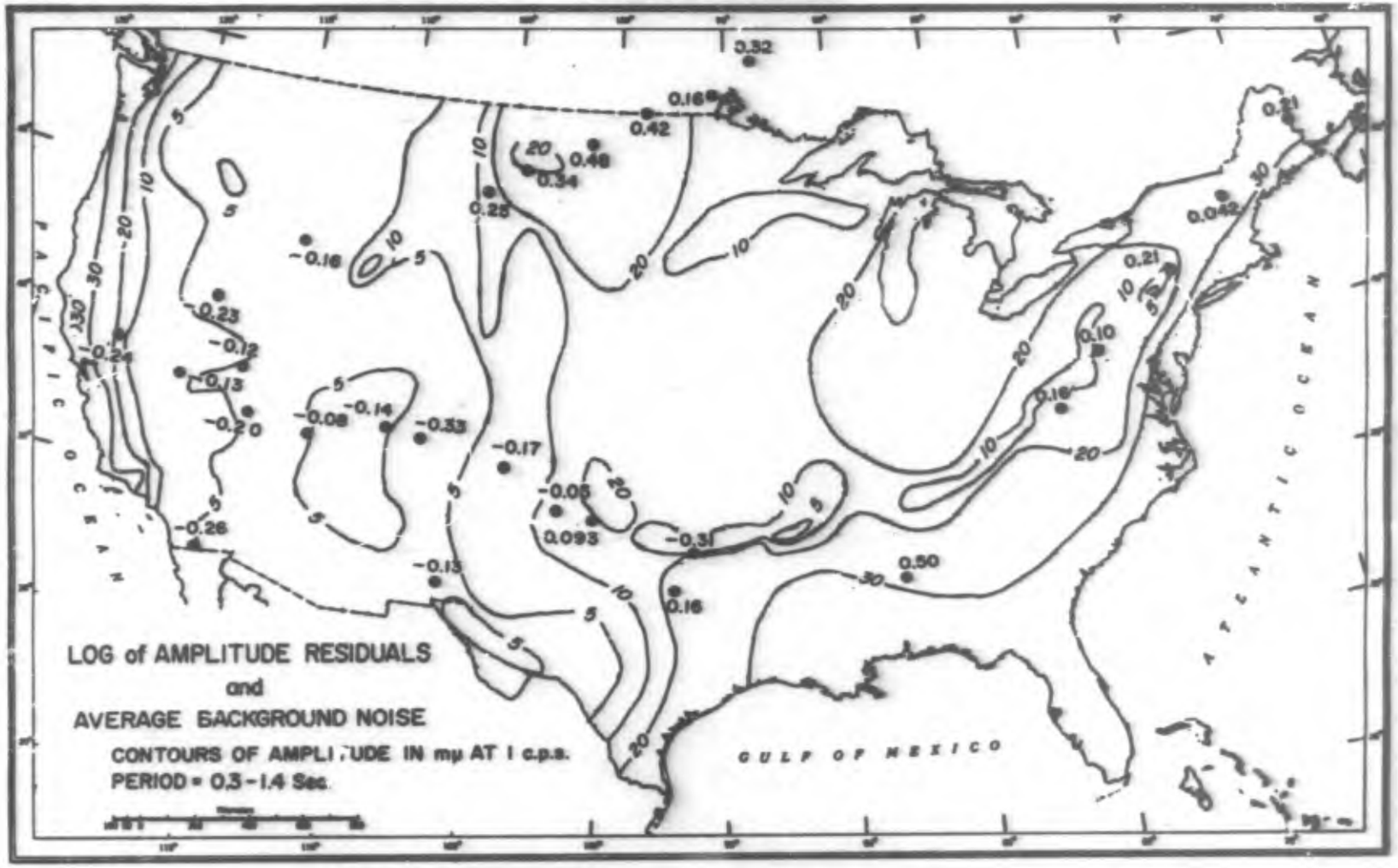
UNITED STATES
LOG of AMPLITUDE RESIDUALS
and
AVERAGE BACKGROUND NOISE
CONTOURS OF AMPLITUDE IN mμ AT 1 c.p.s.
PERIOD = 0.3 - 1.4 Sec.
GULF OF MEXICO
ATLANTIC OCEAN

Figure 17

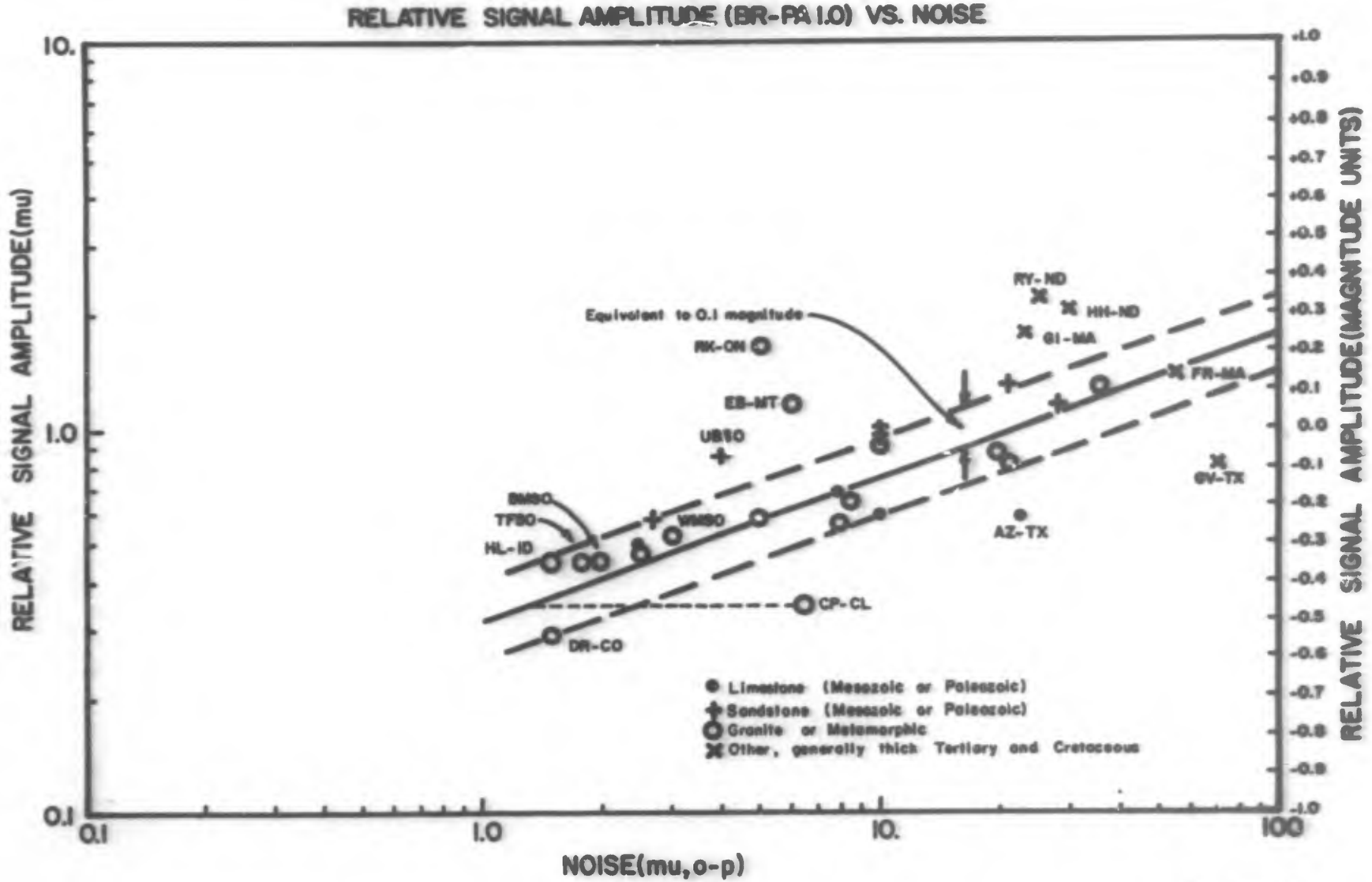
RELATIVE SIGNAL AMPLITUDE (BR-PA 1.0) VS. NOISE
RELATIVE SIGNAL AMPLITUDE(mu)
RELATIVE SIGNAL AMPLITUDE(MAGNITUDE UNITS)
NOISE(mu,o-p)
10.
1.0
0.1
0.1
1.0
10.
100
+1.0
+0.9
+0.8
+0.7
+0.6
+0.5
+0.4
+0.3
+0.2
+0.1
0.0
-0.1
-0.2
-0.3
-0.4
-0.5
-0.6
-0.7
-0.8
-0.9
-1.0
Equivalent to 0.1 magnitude
RK-ON
EB-MT
UBSO
BMSO
TFSO
HL-ID
WMSO
CP-CL
DR-CO
RY-ND
HH-ND
GI-MA
FR-MA
GV-TX
AZ-TX
Limestone (Mesozoic or Paleozoic)
Sandstone (Mesozoic or Paleozoic)
Granite or Metamorphic
Other, generally thick Tertiary and Cretaceous

Figure 18

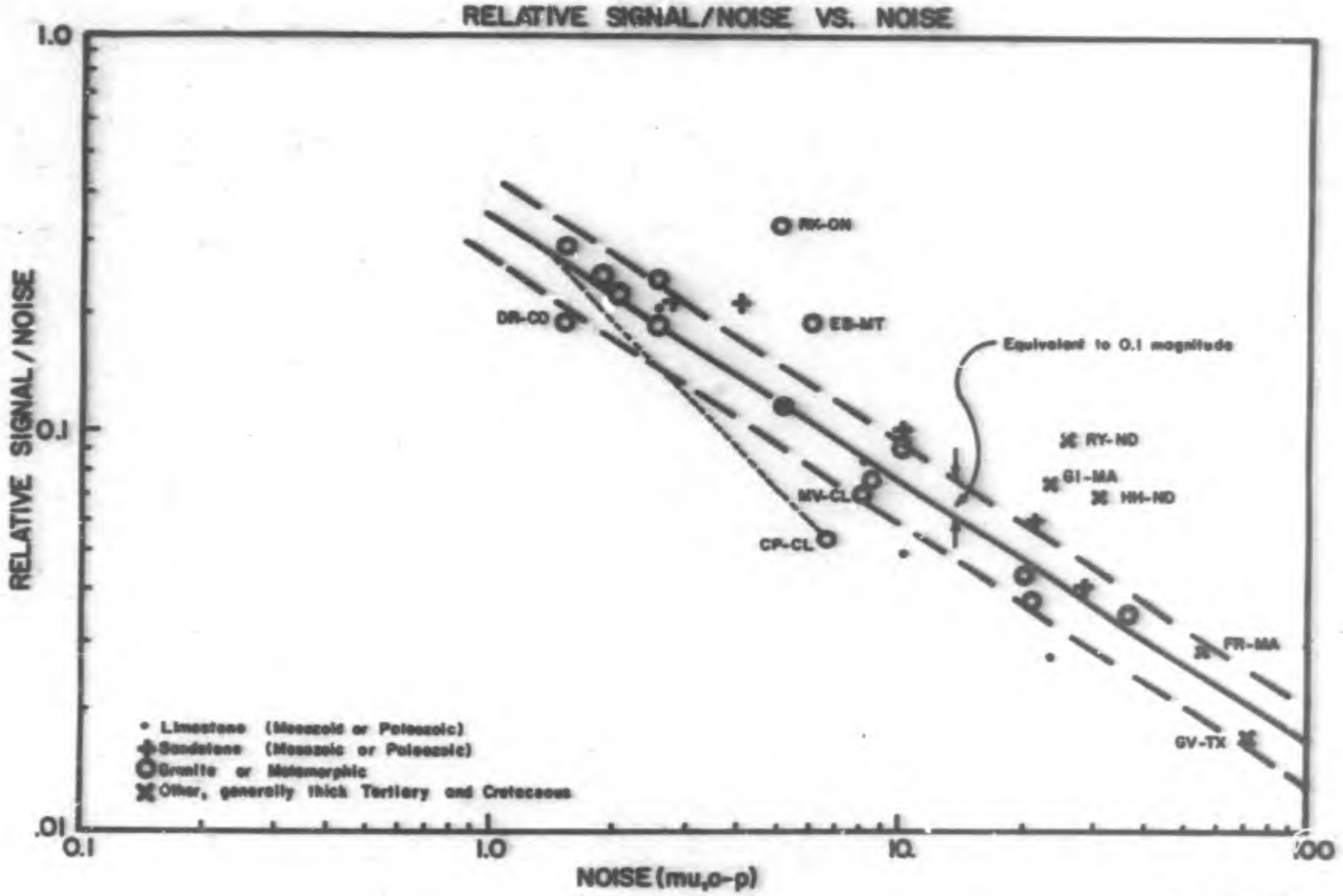
RELATIVE SIGNAL/NOISE VS. NOISE
1.0
0.1
.01
RELATIVE SIGNAL / NOISE
0.1
1.0
10.
NOISE (mu,σ-p)
RK-ON
EB-MT
DR-CO
Equivalent to 0.1 magnitude
RY-ND
GI-MA
HH-ND
MV-CL
CP-CL
FR-MA
GV-TX
Limestone (Mesozoic or Paleozoic)
Sandstone (Mesozoic or Paleozoic)
Granite or Metamorphic
Other, generally thick Tertiary and Cretaceous

Figure 19

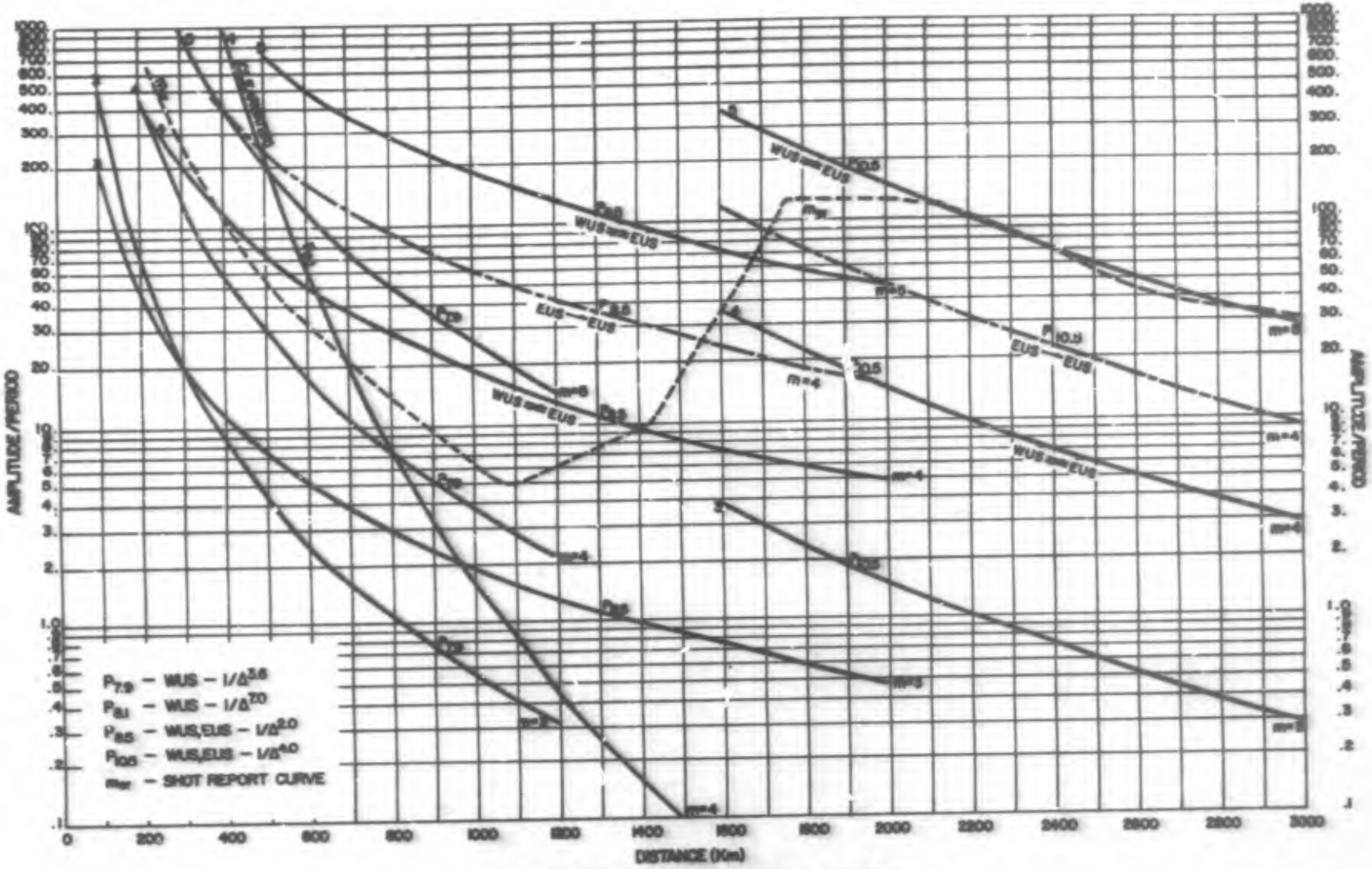

AMPLITUDE/PERIOD vs EPICENTRAL DISTANCE
vs MAGNITUDE (m)

Figure 20

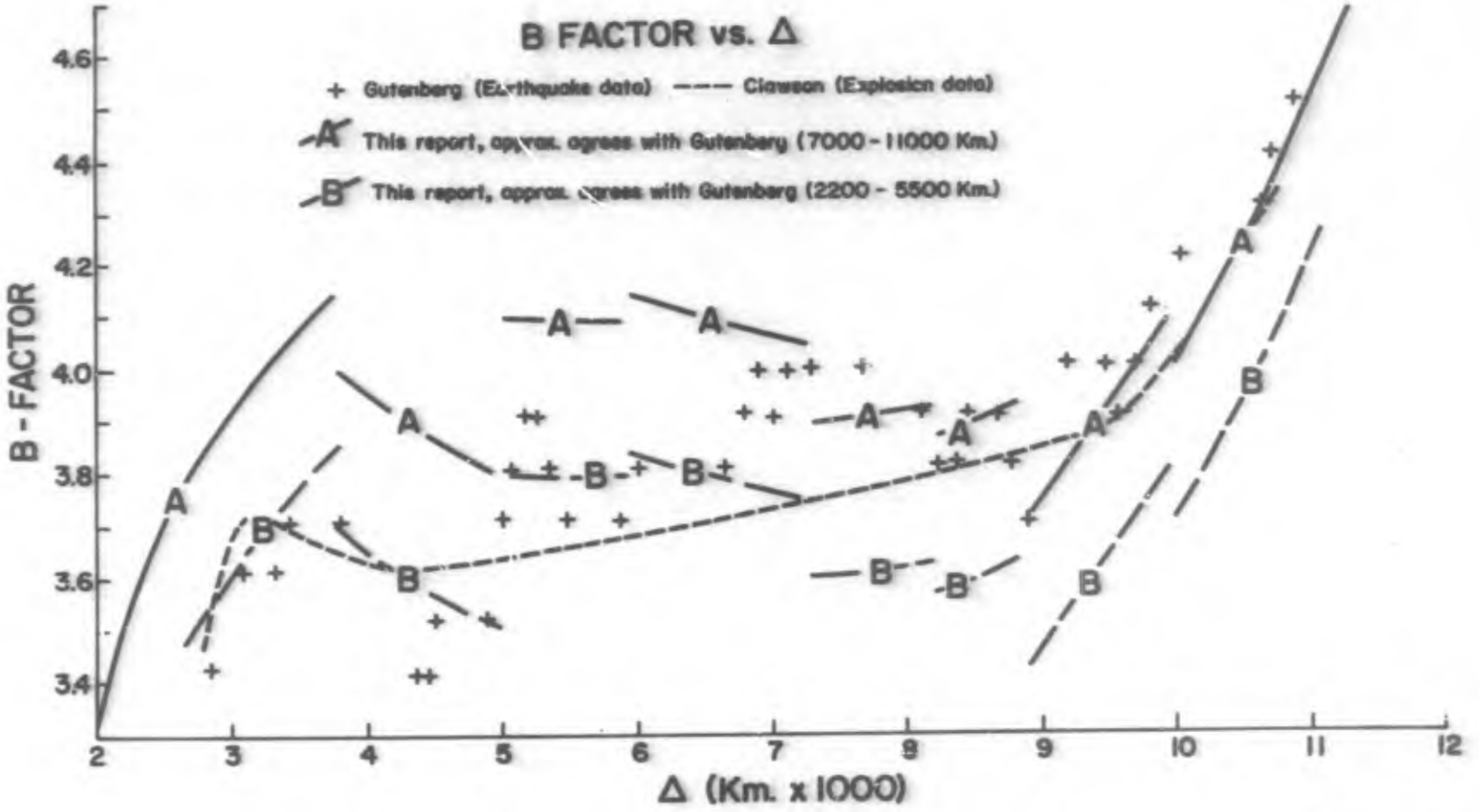
B FACTOR vs. Δ
+ Gutenberg (Earthquake data) ---- Clawson (Explosion data)
A This report, approx. agrees with Gutenberg (7000 - 11000 Km.)
B This report, approx. agrees with Gutenberg (2200 - 5500 Km.)
B - FACTOR
4.6
4.4
4.2
4.0
3.8
3.6
3.4
2
3
4
5
6
7
8
9
10
11
12
Δ (Km. x 1000)

Figure 21

Unclassified
Security Classification

DOCUMENT CONTROL DATA - R&D

(Security classification of title, body of abstract and indexing annotation must be entered when the overall report is classified)

1. ORIGINATING ACTIVITY (Corporate author)
TELEDYNE INDUSTRIES, INC.
ALEXANDRIA, VIRGINIA

2a. REPORT SECURITY CLASSIFICATION
Unclassified

2b. GROUP

3. REPORT TITLE
INVESTIGATION OF P TRAVEL-TIME CURVE

4. DESCRIPTIVE NOTES (Type of report and inclusive dates)
Scientific

5. AUTHOR(S) (Last name, first name, initial)
Evernden, J.F.; Clark, D.M.

6. REPORT DATE
29 July 1969

7a. TOTAL NO. OF PAGES
91

7b. NO. OF REFS

8a. CONTRACT OR GRANT NO.
F33657-69-C-0913 ✓

8b. PROJECT NO.
VELA T/9706
ARPA Order No. 624
ARPA Program Code No. 9F10

9a. ORIGINATOR'S REPORT NUMBER(S)
236

9b. OTHER REPORT NO(S) (Any other numbers that may be assigned this report)

10. AVAILABILITY/LIMITATION NOTICES
This document is subject to special export controls and each transmittal to foreign governments or foreign nationals may be made only with prior approval of Chief, AFTAC.

11. SUPPLEMENTARY NOTES

12. SPONSORING MILITARY ACTIVITY
ADVANCED RESEARCH PROJECTS AGENCY
NUCLEAR MONITORING RESEARCH OFFICE
WASHINGTON, D. C.

13. ABSTRACT

By using a large number of LRSM stations and a number of earthquakes from all azimuths and the well controlled nuclear explosions, a study of the "P" travel-time curve reveals it to be nearly a series of straight-lines or legs throughout the total distance of about 105° (degrees). Time as well as amplitude residuals were determined for the stations used and were found to be acceptably consistent. Analysis of the variance of the several modes of handling the data of each leg is shown which is significant in indicating the relative probability of each model as an explanation of the observed data. The "F" statistic value, degrees of freedom, etc. are shown for each leg. The existence of real differences in "P" travel-times and thus of mantle velocity structure are illustrated indicating that the velocity varies as a function of azimuth.

The very close correlation between site geology and average noise level on signal amplitude is discussed as well as this effect on magnitude calculations.

In addition, a computed "B-factor" curve developed from this study is compared with Gutenberg's and one by Clawson of Geotech.

14. KEY WORDS
Segmented travel-time curve
LRSM and arrays
"B" factor

Unclassified